

1 On the interpretation of inter-model spread in CMIP5 climate sensitivity 2 estimates

3 Jessica Vial · Jean-Louis Dufresne · Sandrine Bony

4
5 Received: date / Accepted: date

6 **Abstract** This study diagnoses the climate sensitivity, radiative forcing and climate feedback estimates from
7 eleven general circulation models participating in the Fifth Phase of the Coupled Model Intercomparison Project
8 (CMIP5), and analyzes inter-model differences. This is done by taking into account the fact that the climate
9 response to increased carbon dioxide (CO_2) is not necessarily only mediated by surface temperature changes, but
10 can also result from fast land and tropospheric adjustments to the CO_2 radiative forcing. By considering
11 tropospheric adjustments to CO_2 as part of forcings rather than feedbacks, and by using the radiative kernels
12 approach, we decompose climate sensitivity estimates in terms of feedbacks and adjustments associated with
13 water vapor, temperature lapse rate, surface albedo and clouds. Taking tropospheric adjustments into account
14 reduces the strength of cloud feedbacks by about 33% on average, but does not affect much the spread of model
15 estimates. The inter-model spread of climate sensitivity estimates primarily results from differing climate
16 feedbacks. About 70% of the spread stems from cloud feedbacks, with a large contribution from the tropics.
17 Differences in tropical cloud feedbacks between low-sensitivity and high-sensitivity models occur over a large
18 range of dynamical regimes, but primarily arise from the regimes associated with a predominance of shallow
19 cumulus and stratocumulus clouds. The combined water vapor plus lapse rate feedback also contributes to the
20 spread of climate sensitivity estimates, with inter-model differences arising primarily from the relative humidity
21 responses throughout the troposphere.

22 Finally, this study points to a substantial role of nonlinearities in the calculation of adjustments and feedbacks
23 for the interpretation of inter-model spread in climate sensitivity estimates. We show that in climate model
24 simulations with large forcing (e.g., $4 \times CO_2$), nonlinearities cannot be assumed minor and neglected. Having said
25 that, some results presented here are consistent with a number of previous feedback studies, despite the very
26 different nature of the methodologies and all the uncertainties associated with them.

27
28 **Keywords** Climate sensitivity · feedback · radiative forcing · fast adjustment · radiative kernel · CMIP5 climate
29 model simulations · climate change · inter-model spread

30 1 Introduction

31 The equilibrium global-mean surface temperature change associated with a doubling of CO₂ concentration in the
32 atmosphere is referred to as Climate Sensitivity. As it controls many aspects of climate change, including the
33 response of the hydrological cycle and of regional climate features to anthropogenic activities, climate sensitivity
34 remains a centrally important measure of the size, and significance, of the climate response to greenhouse gases
35 (Bony et al, 2013, in press). Unfortunately, climate sensitivity estimates from climate models have long been
36 associated with a large spread (Charney et al, 1979; Randall et al, 2007). This spread, which has not narrowed
37 among the current generation of models (Andrews et al, 2012), remains within the 2 to 4.5 degrees range.

38 Attempts to estimate the likely range of climate sensitivity from observations of the current climate or from instru-
39 mental or natural archives have not narrowed this range substantially (Knutti and Hegerl, 2008). An alternative
40 to this holistic approach consists in constraining observationally the individual processes or feedbacks that con-
41 trol climate sensitivity, especially those which are most responsible for inter-model differences. For this purpose,
42 interpreting the spread of climate sensitivity estimates amongst models constitutes a pre-requisite.

43 For climate models participating in the Third Phase of the Coupled Model Intercomparison Project (CMIP3),
44 cloud feedbacks were identified as the leading source of spread of climate sensitivity estimates (Bony et al, 2006;
45 Dufresne and Bony, 2008; Soden and Held, 2006), with a major contribution from low-cloud feedbacks (Bony and
46 Dufresne, 2005; Randall et al, 2007; Webb et al, 2006). However, Gregory and Webb (2008) and Andrews and
47 Forster (2008) subsequently pointed out that the atmosphere, humidity and clouds in particular, could exhibit
48 fast adjustments to the CO₂ radiative forcing, and that inter-model differences in cloud adjustments could
49 contribute significantly to the spread of climate sensitivity.

50 The CO₂ radiative forcing has been commonly taken as the radiative flux change at the top of the atmosphere
51 (TOA) after allowing the stratosphere to adjust to the CO₂ increase (Forster et al, 2007). The reason for using
52 this stratosphere-adjusted forcing rather than the instantaneous CO₂ forcing, is that the stratospheric
53 temperature adjustment occurs on a much smaller time-scale (i.e., weeks to months) than the long-term climate
54 response (operating over at least several decades). The same rationale is used now for the tropospheric
55 adjustments to change in CO₂ concentration. As tropospheric adjustments to greenhouse gases are fast and not
56 necessarily mediated by surface temperature changes, they may not be considered as part of feedbacks but rather
57 as part of forcings. Such a distinction matters for models for which the cloud response to increased CO₂ does not
58 exhibit much correlation with surface warming but primarily results from fast tropospheric adjustments. These
59 findings call for a revisit of the concepts of forcing and feedback, of the methodologies used to assess them from
60 model outputs, and of our interpretation of climate sensitivity uncertainties.

61

62 The purpose of this study is to interpret the range of equilibrium climate sensitivity estimates from models
63 participating in the Fifth Phase of the Coupled Model Intercomparison Project (CMIP5, Taylor et al, 2012). In
64 section 2, we present the methodologies used to diagnose the radiative forcings and feedbacks of each model by
65 taking into account the tropospheric and land surface adjustments to CO₂. In section 3, these methodologies are
66 applied to CMIP5 model outputs, and model estimates of climate sensitivity are interpreted in terms of radiative
67 adjustments and feedbacks. The inter-model spread of climate sensitivity is quantified, and then decomposed into

68 different contributions related to individual adjustments and feedbacks, and into regional contributions. As the
 69 spread of climate sensitivity arises primarily from the tropics, we analyze in section 4 inter-model differences in
 70 water vapor, lapse-rate and cloud feedbacks. A conclusion is presented in section 5.

71 2 Data and Methodology

72 2.1 Conceptual framework

73 Let F and ΔR (in Wm^{-2}) be a radiative forcing imposed to the climate system and the resulting imbalance in
 74 the Earth's radiation budget at the TOA, respectively. The climate system responds to this radiative imbalance
 75 by changing its global mean surface temperature ΔT_s (in Kelvin), and at any time the climate response opposes
 76 the radiative forcing according to:

$$\Delta R = F + \lambda \Delta T_s, \quad (1)$$

77 where λ (< 0 , in $Wm^{-2}K^{-1}$) is the feedback parameter (Bony et al, 2006; Dufresne and Bony, 2008; Gregory et al,
 78 2004).

79 When the climate system reaches a new equilibrium, $\Delta R = 0$ and the equilibrium climate sensitivity ΔT_s^e can be
 80 estimated as

$$\Delta T_s^e = \frac{-F}{\lambda} \quad (2)$$

81 Consider now that the radiative forcing F induces tropospheric adjustments to increased CO_2 concentration
 82 ($F_{adj,co2}$), without any change in ΔT_s . The equilibrium climate sensitivity $\Delta T_s^{e'}$ can then also be estimated as:

$$\Delta T_s^{e'} = \frac{-(F + F_{adj,co2})}{\lambda'}, \quad (3)$$

83 where λ' is the feedback parameter when the adjustments are considered as part of the forcing.

84 If we assume that both equilibrium temperature changes are equals (i.e., $\Delta T_s^e = \Delta T_s^{e'}$), then the relationship
 85 between λ and λ' can be written as:

$$\frac{\lambda'}{\lambda} = \frac{F + F_{adj,co2}}{F} \quad (4)$$

86 Figure 1, which illustrates this reasoning, shows the relationships between the forcings, the feedback parameters
 87 and the equilibrium global mean surface temperature according to the energy balance in Eq. 1, when the
 88 adjustments to CO_2 are included in the forcing (in blue) or in the feedbacks (in black). As discussed later in this
 89 section and Section 2.2, our attempts to devise a forcing that could capture adjustments to CO_2 without also

90 capturing changes due to land surface warming, were unsuccessful. Figure 1 also represents this forcing (i.e., that
 91 includes adjustments to CO_2 and land surface warming: $F + F_{adj}$), which can, however, easily be diagnosed from
 92 CMIP5 experiments, and that we use in this study (as defined in Section 2.2 and Eq. 12).

93

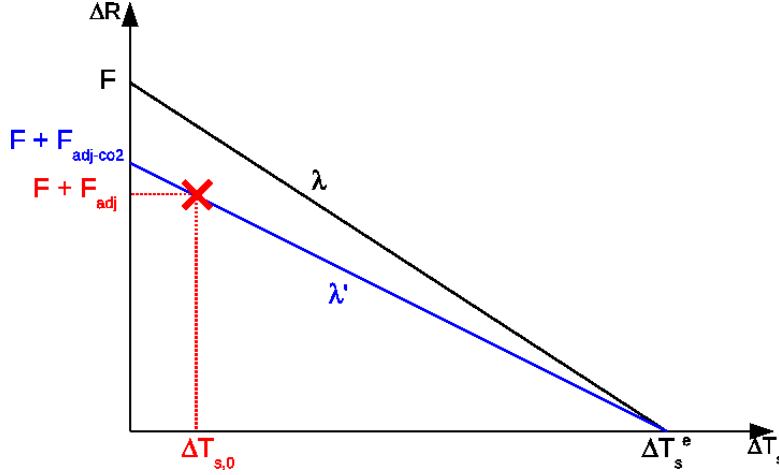


Fig. 1 Schematic representation of Eq. 1 showing the relationships between the forcings, the feedback parameters and the equilibrium global mean surface temperature when the tropospheric adjustments to CO_2 forcing are considered (in blue) or not (in black). Here, we assume that the adjustments to CO_2 are negative ($F_{adj-co2} < 0$). The intercept at $\Delta T_s = \Delta T_{s,0}$ (red cross) represents the adjusted radiative forcing estimated from fixed-SST experiments, in which the land surface temperature is allowed to adjust by $\Delta T_{s,0}$ to increased CO_2 , while holding the SST fixed (see also Section 2.2).

94 Under this framework, the imbalance in the Earth's radiation budget at the TOA (ΔR) depends on changes in
 95 CO_2 concentration, in surface temperature T_s and in the feedback variables X (where $X \equiv \sum x$ and x refers to
 96 atmospheric temperature, water vapor, surface albedo and clouds). At first order, by neglecting nonlinearities, Eq.
 97 1 can be written in a general form as:

$$\Delta R(\text{CO}_2, T_s, X) \approx \left. \frac{\partial R}{\partial \text{CO}_2} \right|_{T_s, X} \Delta \text{CO}_2 + \left. \frac{\partial R}{\partial T_s} \right|_{\text{CO}_2, X} \Delta T_s + \left. \frac{\partial R}{\partial X} \right|_{T_s, \text{CO}_2} \Delta X \quad (5)$$

98 where on the right hand side of Eq. 5, we now explicitly introduce the stratosphere-adjusted forcing to CO_2 (first
 99 term), the Planck response (second term) and the TOA radiative response to changes in feedback variables (third
 100 term). There are at least two more specific approaches that can be used to diagnose the radiative forcings and
 101 feedbacks from Eq. 5.

102

103 **1) In the case where tropospheric adjustments to CO_2 are not taken into account**, but rather included in
 104 the feedback response (e.g., in Soden and Held, 2006), the changes in feedback variables X only depend on surface
 105 temperature T_s , while the dependency to CO_2 is neglected: $\Delta X \equiv \Delta X(T_s) \approx \frac{\partial X}{\partial T_s} \Delta T_s$.

106 Eq. 5 can then be re-written as:

$$\Delta R(\text{CO}_2, T_s, X(T_s)) \approx \left. \frac{\partial R}{\partial \text{CO}_2} \right|_{T_s, X} \Delta \text{CO}_2 + \left[\left. \frac{\partial R}{\partial T_s} \right|_{\text{CO}_2, X} + \left. \frac{\partial R}{\partial X} \right|_{T_s, \text{CO}_2} \frac{\partial X}{\partial T_s} \right] \Delta T_s \quad (6)$$

107 **2) In the case where we recognize the existence of tropospheric adjustments to CO_2** while holding the SST
 108 fixed, but allowing the land surface temperature to adjust, ΔT_s can be decomposed as:

$$\Delta T_s = \Delta T_{s,0} + \Delta T_{s,\Delta SST} \quad (7)$$

109 where $\Delta T_{s,0}$ is the surface temperature change after CO_2 quadrupling at fixed SST and $\Delta T_{s,\Delta SST}$ is the subsequent
 110 surface temperature change when the SST varies by ΔSST .

111 The changes in the variables X now depend on both surface temperature and CO_2 changes as follows:

$$\Delta X \equiv \Delta X(CO_2, T_s) \approx \left. \frac{\partial X}{\partial CO_2} \right|_{T_s} \Delta CO_2 + \left. \frac{\partial X}{\partial T_s} \right|_{CO_2} \Delta T_{s,0} + \left. \frac{\partial X}{\partial T_s} \right|_{CO_2} \Delta T_{s,\Delta SST} \quad (8)$$

112 This yields for Equation 5:

$$\begin{aligned} \Delta R(CO_2, T_s, X(CO_2, T_s)) \approx & \left[\left. \frac{\partial R}{\partial CO_2} \right|_{T_s, X} + \left. \frac{\partial R}{\partial X} \right|_{T_s, CO_2} \left. \frac{\partial X}{\partial CO_2} \right|_{T_s} \right] \Delta CO_2 \\ & + \left[\left. \frac{\partial R}{\partial T_s} \right|_{CO_2, X} + \left. \frac{\partial R}{\partial X} \right|_{T_s, CO_2} \left. \frac{\partial X}{\partial T_s} \right|_{CO_2} \right] \Delta T_{s,0} \\ & + \left[\left. \frac{\partial R}{\partial T_s} \right|_{CO_2, X} + \left. \frac{\partial R}{\partial X} \right|_{T_s, CO_2} \left. \frac{\partial X}{\partial T_s} \right|_{CO_2} \right] \Delta T_{s,\Delta SST} \end{aligned} \quad (9)$$

113 The right hand side of this equation includes the stratosphere- and troposphere-adjusted forcing to CO_2 (first
 114 row), the fast climate response to a change in land surface temperature (second row), and the climate response
 115 to the subsequent temperature change when the oceans warm (third row).

116 In this present study, we follow this approach to diagnose the radiative forcings and feedbacks. The next section
 117 describes how we proceed, in practice, when we apply this methodology to CMIP5 model experiments.

118

119 2.2 Using CMIP5 experiments to diagnose radiative forcings and feedbacks

120 We analyze climate model outputs recently made available on the CMIP5 multi-model ensemble archive (<http://pcmdi3.llnl.gov/esgcat/home.htm>). The list of models (and institutions) considered in this study is given in
 121 Table 1.
 122

123

124 Model outputs from a range of CMIP5 idealized experiments (described in Taylor et al, 2012) are analyzed:

- 125 1. abrupt4xCO2, a fully-coupled ocean-atmosphere simulation in which the CO_2 concentration is abruptly quadru-
 126 pled and then held fixed
- 127 2. sstClim, a 30-year atmosphere-only experiment forced by a prescribed climatology of sea surface temperatures
 128 (SSTs) derived from fully-coupled pre-industrial simulation (piControl)

	Model acronym	Institution	Climate sensitivity for $2\times\text{CO}_2$ (in K)
1	IPSL-CM5A-LR	Institut Pierre-Simon Laplace, France	3.9
2	NorESM1-M	Norwegian Climate Center, Norway	2.7
3	MPI-ESM-LR	Max Planck Institute for Meteorology, Germany	3.7
4	INMCM4	Institute for Numerical Mathematics, Russia	1.9
5	HadGEM2-ES	Met Office Hadley Centre, United Kingdom	4.4
6	CanESM2	Canadian Centre for Climate Modelling and Analysis, Canada	3.7
7	MIROC5	Japan Agency for Marine-Earth Science and Technology, Japan	2.8
8	CCSM4	National Center for Atmospheric Research, United States	2.3
9	BNU-ESM	College of Global Change and Earth System Science, Beijing Normal University, China	4.1
10	FGOALS-s2	State Key Laboratory of Numerical Modeling for Atmospheric Sciences and Geophysical Fluid Dynamics, Institute of Atmospheric Physics, Chinese Academy of Sciences, Beijing, China	4.1
11	MRI-CGCM3	Meteorological Research Institute, Japan	2.6

Table 1 Institute, model name and climate sensitivity (computed from Eqs. 22-29) of the 11 CMIP5 Global Climate Models (GCMs) considered in this study.

129 3. sstClim4xCO2, the same experiment as sstClim, except that the CO₂ concentration is abruptly quadrupled
130 and maintained fixed for 30 years.

131 We compute monthly-resolved seasonal cycle using the 30-year periods of the sstClim and sstClim4xCO2
132 experiments and a 10-year period centered around the 130th year after the CO₂ quadrupling in abrupt4xCO2. For
133 the 3D fields, we use the data on pressure levels.

134

135 The framework described in the previous section provides the possibility of isolating the role of CO₂ and surface
136 warming in the radiative changes associated with clouds, water vapor, albedo and temperature (Eq. 9).
137 Technically, however, it is not possible, using this set of experiments, to separate the climate response to land
138 surface warming (second row in Eq. 9) from the tropospheric adjustments to CO₂ (first row in Eq. 9).

139 In the sstClim4xCO2 experiment, the atmosphere and land surface are free to respond to the change in CO₂
140 concentration. However, the climate feedbacks, which by definition are mediated by the global mean surface
141 temperature change, are prevented from evolving, since the fixed-SST condition implies that $\Delta T_s \simeq 0$ (actually,
142 the small change in T_s resulting from the warming of land surfaces, $\Delta T_{s,0}$, is of the order of 0.5 K). Therefore,
143 the fixed-SST experiments we dispose, only allow us to consider the adjustments to CO₂ and land surface
144 warming together. According to Eq. 1, the atmosphere-adjusted radiative forcing F' , as defined in Eq. 12, is
145 simply the change in the net TOA radiation fluxes between the 30-year average climate of sstClim4xCO2 and
146 sstClim experiments (i.e., $F' = \Delta R$).

147 As for the radiative feedbacks (third row in Eq. 9), they are investigated between the sstClim4xCO2 and
148 abrupt4xCO2 experiments, where the CO₂ concentration is now held fixed, but the surface temperature is
149 allowed to change as the ocean warms.

150

151 Some previous studies have attempted to consider the radiative changes due to land surface warming as part of
152 the climate response rather than of the forcings (Hansen et al, 2005; Mauritsen et al, submitted). This was done
153 by assuming that the global climate feedback parameter is the same in a fixed-SST experiment as in a transient
154 experiment (i.e., $\frac{\partial R}{\partial T_s} \Big|_{\text{CO}_2, X} + \frac{\partial R}{\partial X} \Big|_{T_s, \text{CO}_2} \frac{\partial X}{\partial T_s} \Big|_{\text{CO}_2}$ in Eq. 9 is constant). This is very unlikely since, as explained
155 previously, in a fixed-SST experiment most feedbacks (if not all) are largely inhibited over the oceans. But the
156 main reason why it is not appropriate to make this assumption here is that although the global climate feedback

157 parameter might be independent of climate state at first order, this is not necessarily true regionally nor for
 158 individual feedbacks (Boer and Yu, 2003).

159 We therefore diagnose the radiative forcing by permitting the stratospheric temperature, the troposphere and the
 160 land surface temperatures to adjust to the increased CO_2 concentration. And since the climate feedbacks are
 161 delayed by century time-scales because of the ocean’s thermal inertia, it is not unreasonable to include “fast
 162 processes”, such as land and sea-ice surface warming, withing the forcing rather than in the long-term climate
 163 response.

164
 165 Hereafter, and to ensure clarity throughout this paper, the different terms in Equation 9 are defined as:

the stratosphere-adjusted forcing to CO_2 :

$$F = \left. \frac{\partial R}{\partial CO_2} \right|_{T_s, X} \Delta CO_2 \quad (10)$$

the tropospheric adjustments to CO_2 forcing and land surface warming:

$$F_{adj} = \left. \frac{\partial R}{\partial X} \right|_{T_s, CO_2} \frac{\partial X}{\partial CO_2} \Delta CO_2 + \left[\left. \frac{\partial R}{\partial T_s} \right|_{CO_2, X} + \left. \frac{\partial R}{\partial X} \right|_{T_s, CO_2} \frac{\partial X}{\partial T_s} \right] \Delta T_{s,0} \quad (11)$$

the atmosphere-adjusted forcing to CO_2 and land surface warming:

$$F' = F + F_{adj} \quad (12)$$

the Planck response:

$$\lambda_p = \left. \frac{\partial R}{\partial T_s} \right|_{CO_2, X} \quad (13)$$

the feedback parameter including the Planck response:

$$\lambda' = \lambda_p + \left. \frac{\partial R}{\partial X} \right|_{T_s, CO_2} \frac{\partial X}{\partial T_s} \quad (14)$$

166
 167
 168 In the following sections 2.3, 2.4 and 2.6, we describe how the tropospheric adjustments to CO_2 (Eq. 11) and the
 169 feedbacks (Eq. 18) are computed using the radiative kernel approach, and how the climate sensitivities (in Table
 170 1) are estimated within that framework.

172 2.3 Estimate of adjustments

173 Here, the tropospheric adjustments to CO₂ and land surface warming arise, to first order, from
 174 changes in temperature (t), water vapor (wv), surface albedo (alb) and cloud (cl), which are induced
 175 by increased CO₂ and land surface warming, but without any change in sea surface temperature:
 176 $F_{adj} = \sum_x F_x + Re^f = F_t + F_{wv} + F_{alb} + F_{cl} + Re^f$ (Eq. 11), where Re^f is a residual term, usually neglected for
 177 sufficiently small climate perturbations (e.g., Soden et al, 2008). However, in large forcing experiments (e.g.,
 178 $4 \times CO_2$), this residual term is sometimes too large to be ignored; this drawback of the kernel technique is
 179 discussed in more details in section 2.5.

180
 181 Following the same approach as for the feedback estimation (in section 2.4 - see also in Soden et al, 2008), all
 182 clear- and all-sky adjustment terms (except clouds) are derived using the radiative kernel technique as follow:

$$F_x = \frac{\partial R}{\partial x} \Delta x = K_x \Delta x, \quad (15)$$

183 where K_x is the radiative kernel (in Wm^{-2} by unit of x). We use the same kernels as in Shell et al (2008), the
 184 National Center for Atmospheric Research (NCAR) model's kernels for water vapor, temperature and albedo,
 185 which are made available at <http://people.oregonstate.edu/~shellk/kernel.html>. Each kernel, K_x , is obtained
 186 by perturbing the climate base state (with pre-industrial CO₂ concentration) by a standard anomaly δx of the
 187 corresponding climate variable x at each grid point and model level and by measuring the resulting change in
 188 TOA radiative fluxes (with separate consideration of the all- and clear-sky LW and SW radiation fluxes). See
 189 Soden et al (2008) and Shell et al (2008) for more details on the kernel technique.

190 Δx is the climate response of each variable, computed by difference between the 30-year model predicted climate
 191 in sstClim4xCO2 and the 30-year climate of the sstClim simulation (refer to section 2.2 for details on the
 192 experiments). Both K_x and Δx are functions of longitude, latitude, pressure level and are monthly means. To
 193 obtain tropospheric averages, the water vapor and temperature adjustments are vertically integrated (by
 194 summing over mass-weighted model levels) up to the tropopause level, which varies linearly between 300 hPa at
 195 the poles and 100 hPa at the equator. As commonly done in feedback studies, the temperature radiative response
 196 is further separated into the Planck response to land surface warming (F_p) and the lapse rate (F_{lr}).

197
 198 The cloud adjustment is estimated by the changes in cloud radiative effect (CRE) and corrected for changes in
 199 non-cloud variables that can alter the change in CRE and lead to a biased estimate of the cloud adjustment.

$$F_{cl} = \Delta R - \Delta R^0 - \left[\sum_x (F_x - F_x^0) + (G - G^0) \right], \quad (16)$$

200 where the exponent ⁰ indicates clear-sky variables, and ΔR is computed with the same experiments as Δx (i.e.,
 201 between sstClim4xCO2 and sstClim). G and G^0 are the all-sky and clear-sky stratosphere-adjusted forcing

202 computed at the tropopause, for a quadrupling CO_2 , using the Laboratoire de Météorologie Dynamique (LMDz)
 203 radiation code and control climate state. $G - G^0$ is the cloud masking effect arising from changes in CO_2
 204 concentration only, estimated at about $-1.24 Wm^{-2}$. This yields a proportionality of cloud masking of
 205 $\frac{G - G^0}{G} \sim -0.16$, which is consistent with that reported in Soden et al (2008).

206

207 Finally, the magnitude of the residual term Re^f (in Wm^{-2} , reported for each model in Table 2) is computed
 208 for clear-sky conditions (by construction, it is the same for all-sky conditions) by differencing the clear-sky TOA
 209 radiative fluxes from the sum of the clear-sky adjustment terms and clear-sky CO_2 forcing:

$$Re^f = \Delta R^0 - \left(\sum_x F_x^0 + G^0 \right) = \Delta R^0 - (F_t^0 + F_{wv}^0 + F_{alb}^0 + G^0) \quad (17)$$

210 In this paper, we often express this quantity in percent as: $\%Re^f = \left| \frac{Re^f}{\Delta R^0} \right| \times 100$ (also reported in Table 2 into
 211 brackets).

212

213 Vertically-integrated, global and annual mean tropospheric adjustments to CO_2 and land surface warming are
 214 shown in Table 2 for each model; multi-model ensemble-mean maps also are presented in Fig. 2. We find a
 215 relatively large negative contribution from the temperature associated with land surface warming (F_p). Clouds
 216 constitute the second most important tropospheric adjustment to CO_2 ; it is positive for most models, dominated
 217 by the shortwave component (F_{clsw}) and stronger over land than over the ocean (Fig. 2d and f). However, the
 218 cloud adjustment is negative over the storm track regions (Fig. 2f, and as reported in Block and Mauritsen,
 219 submitted), with a greater contribution arising from the longwave component (Fig. 2e). Additional analyzes
 220 using aquaplanet experiments ('aquaControl' and 'aqua4xCO2' - not presented in the paper) show that the
 221 positive contribution from the lapse rate (over land - not shown), the water vapor (over land, Fig. 2b) and the
 222 albedo (over sea-ice, northern continental areas and semi-arid regions, Fig. 2c) are due to land surface warming
 223 rather than tropospheric adjustments to CO_2 . On the other hand, cloud changes partly reflect changes in the
 224 large-scale circulation induced by the direct effect of CO_2 , especially the weakening of large-scale ascending
 225 motions over ocean (Bony et al, submitted).

226

227 These adjustment estimates may be compared with values reported in previous studies. For instance, Gregory
 228 and Webb (2008)'s estimates of global cloud adjustments, obtained from the y-intercept of the regression line for
 229 ΔCRE against ΔT_s , are $-1.7 \pm 0.42 Wm^{-2}$ and $0.98 \pm 0.82 Wm^{-2}$ for the LW and SW components, respectively,
 230 of an ensemble of mixed layer ocean models (note that the original $2 \times CO_2$ results have been doubled for ease of
 231 comparison with $4 \times CO_2$ results of this study). While Gregory and Webb (2008)'s and the present estimates are
 232 relatively similar for the SW component, substantial differences arise for the LW cloud adjustment. This can
 233 largely be explained by the cloud-masking effect of non-cloud variables, which is not taken into account in
 234 Gregory and Webb (2008)'s study. Our multi-model mean estimates of the adjustments in CRE (i.e., without the
 235 cloud-masking correction - $[\sum_x (F_x - F_x^0) + (G - G^0)]$ in Eq. 16) are $-1.42 \pm 0.49 Wm^{-2}$ and $0.93 \pm 0.88 Wm^{-2}$

	F_p	F_{lr}	F_{wv}	F_{alb}	F_{clsw}	F_{cllw}	F_{cl}	$\sum_x F_x$	F'	Re^f (% Re^f)
IPSL-CM5A-LR	-1.64	-0.12	0.54	0.18	2.15	-1.33	0.81	-0.21	6.48	-0.77 (10.96)
NorESM1-M	-1.72	-0.04	0.38	0.19	1.61	-0.49	1.09	-0.07	6.95	-0.49 (6.79)
MPI-ESM-LR	-1.58	0.07	0.35	0.15	1.89	-0.43	1.44	0.45	8.63	0.71 (8.39)
INMCM4	-1.45	-0.06	0.55	0.12	-0.32	0.42	0.09	-0.72	6.24	-0.54 (7.26)
HadGEM2	-1.56	0.00	0.28	0.09	1.34	-0.27	1.06	-0.12	6.99	-0.39 (5.50)
CanESM2	-1.52	-0.18	0.40	0.05	1.13	-0.04	1.07	-0.15	7.34	0.02 (0.34)
MIROC5	-1.40	-0.09	0.33	0.16	1.56	-0.66	0.89	-0.09	7.94	0.52 (6.28)
CCSM4	-1.97	0.06	0.39	0.21	1.65	-0.25	1.39	0.11	8.84	1.21 (13.80)
BNU-ESM	-1.37	-0.23	0.56	0.53	1.03	0.07	1.08	0.59	7.87	-0.21 (2.51)
FGOALS-s2	-1.15	-0.33	0.56	0.11	-0.64	0.23	-0.42	-1.22	8.05	1.80 (18.20)
MRI-CGCM3	-1.22	-0.06	0.41	0.16	0.50	0.00	0.49	-0.20	7.19	-0.10 (1.18)
For all models:										
Multi-model mean	-1.51	-0.09	0.43	0.18	1.08	-0.25	0.82	-0.15	7.50	0.16 (7.38)
Inter-model std dev	0.23	0.12	0.10	0.13	0.89	0.48	0.56	0.50	0.84	0.81 (5.38)
For the 8 models that exhibit a linear behavior (i.e., %$Re^f < 10$):										
Multi-model mean	-1.48	-0.07	0.41	0.18	1.09	-0.17	0.90	-0.04	7.39	-0.06 (4.78)
Inter-model std dev	0.15	0.09	0.10	0.15	0.71	0.35	0.42	0.40	0.74	0.46 (3.02)

Table 2 Vertically-integrated (up to tropopause), global and annual mean of adjustments to CO_2 forcing and land surface warming (in Wm^{-2}) estimated using the NCAR model’s radiative kernels, for the 11 CMIP5 models used in this study, their multi-model mean and inter-model standard deviation. Also shown are the multi-model mean and inter-model standard deviation for the 8 models that exhibit a linear behavior in the forcing period (for which % $Re^f < 10$; see also in Section 2.5). From left to right are the contributions from the Planck response to land surface warming (F_p), lapse rate (F_{lr}), water vapor (F_{wv}), albedo (F_{alb}), shortwave, longwave and net cloud components (F_{clsw} , F_{cllw} and F_{cl} , respectively), the sum of all adjustments to CO_2 and land surface warming ($\sum_x F_x$), the total adjusted forcing (F') and the residual term (Re^f , expressed in Wm^{-2} and % Re^f into brackets, expressed in %).

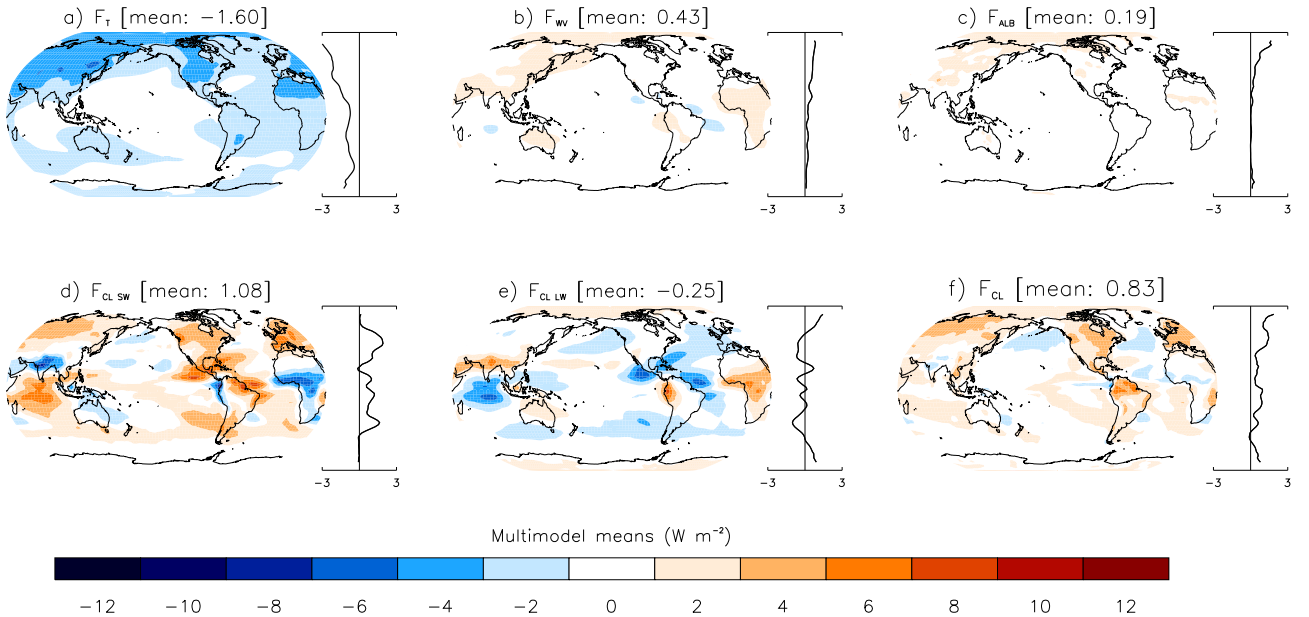


Fig. 2 Multimodel ensemble-mean maps of the tropospheric adjustments associated with temperature (a), water vapor (b), albedo (c) and clouds: shortwave (d), longwave (e) and net component (f) estimated using the NCAR model’s radiative kernels and the sstClim and sstClim4xCO2 experiments. Units in Wm^{-2} .

236 for the LW and SW components, respectively, which are now very similar to Gregory and Webb (2008)’s
 237 estimates. Quantitative differences can also be found by comparing our results with those reported in Colman
 238 and McAvaney (2011). Using the “Partial Radiative Perturbation” technique, Colman and McAvaney (2011)
 239 found that the SW cloud adjustment, estimated at $\sim 1.5 Wm^{-2}$ (scaled by 2 for comparison with $4 \times CO_2$ results
 240 of this study), is the only significant response to CO_2 , while the linear regression highlights additional

241 contributions from the LW cloud adjustment ($\sim -0.2 \text{ Wm}^{-2}$, scaled by 2) and water vapor ($\sim -0.6 \text{ Wm}^{-2}$,
 242 scaled by 2). The different results found by these studies highlight the sensitivity of adjustments to CO_2 to the
 243 methodology employed. Having said that, previous studies' estimates and ours remain qualitatively consistent.

244

245 2.4 Estimate of feedbacks

246 At first order, by neglecting interactions between variables, the feedback parameter, previously defined in Eq. 1
 247 and Eq. 18, is commonly split as the sum of the temperature (t), water vapor (wv), surface albedo (alb) and
 248 cloud (cl) feedback parameters (Bony et al, 2006; Soden et al, 2008), with a longwave (LW) and (SW) radiation
 249 contribution for the water vapor and cloud feedbacks. In addition, here, we consider a residual term Re^λ , which
 250 reflects nonlinearities in the relationship between the TOA radiative flux changes and the climate responses (as
 251 for the adjustments in section 2.3): $\lambda = \sum_x \lambda_x + Re^\lambda = \lambda_t + \lambda_{wv} + \lambda_{alb} + \lambda_{cl} + Re^\lambda$.

252

253 As for the adjustments, all clear- and all-sky feedbacks (except the cloud feedback) are computed using the radiative
 254 kernel technique as follow:

$$\lambda_x = \frac{\partial R}{\partial x} \frac{\Delta x}{\Delta T_{s, \Delta sst}} \quad (18)$$

255 where Δx and $\Delta T_{s, \Delta sst}$ are computed by differencing the 10-year average (centered around the 130th year) model
 256 predicted climate in abrupt4xCO2 from the 30-year climate of the sstClim4xCO2 simulation. By only considering
 257 the period between the abrupt4xCO2 and sstClim4xCO2 experiments, feedbacks are separated from tropospheric
 258 adjustments to CO_2 , and only depend on the surface temperature change when the oceans warm.

259 To obtain tropospheric averages, the water vapor and temperature feedbacks are vertically integrated in the
 260 same way as for the tropospheric adjustments (see Section 2.3). We also separate the temperature feedback into
 261 the lapse rate component (λ_{lr}) and the Planck response (λ_p).

262

263 As for the cloud feedback, we use the same approach as in Soden et al (2008), by estimating the changes in CRE
 264 and correcting for non-cloud feedbacks.

$$\frac{\Delta CRE}{\Delta T_{s, \Delta sst}} = \frac{\Delta R - \Delta R^0}{\Delta T_{s, \Delta sst}} \quad (19)$$

$$\lambda_{cl} = \frac{\Delta CRE}{\Delta T_{s, \Delta sst}} - \sum_x (\lambda_x - \lambda_x^0), \quad (20)$$

265 ΔR and ΔR^0 are with the same experiments as λ_x (i.e., between abrupt4xCO2 and sstClim4xCO2), and the
 266 exponent ⁰ indicates clear-sky variables. As there is no change in forcing between these experiments, the forcing

	λ_p	λ_{lr}	λ_{wv}	λ_{wv+lr}	λ_{alb}	$\lambda_{cls w}$	$\lambda_{clt w}$	λ_{cl}	$\lambda_{wv+lr+alb+cl}$	Re^λ ($\%Re^\lambda$)
IPSL-CM5A-LR										
GFDL	-3.29	-0.97	1.86	0.89	0.18	0.81	0.38	1.18	2.23	0.03 (1.92)
NCAR	-3.27	-0.97	1.94	0.97	0.16	0.89	0.32	1.21	2.32	-0.03 (1.57)
Diff	0.01	0.01	0.08	0.08	0.02	0.08	0.06	0.03	0.08	0.06
NorESM1-M										
GFDL	-3.19	-0.47	1.54	1.07	0.30	-0.14	0.29	0.14	1.47	0.16 (12.67)
NCAR	-3.16	-0.46	1.59	1.13	0.26	-0.04	0.23	0.18	1.53	0.07 (5.45)
Diff	0.04	0.01	0.05	0.05	0.04	0.10	0.06	0.04	0.05	0.09
MPI-ESM-LR										
GFDL	-3.27	-0.88	1.76	0.89	0.29	0.01	0.46	0.45	1.61	0.28 (22.11)
NCAR	-3.24	-0.87	1.83	0.96	0.25	0.12	0.40	0.51	1.68	0.18 (13.88)
Diff	0.03	0.00	0.07	0.07	0.05	0.11	0.06	0.05	0.08	0.11
INMCM4										
GFDL	-3.24	-0.67	1.62	0.95	0.33	-0.20	0.16	-0.05	1.20	0.06 (4.24)
NCAR	-3.20	-0.66	1.68	1.02	0.29	-0.09	0.10	0.00	1.28	-0.05 (3.22)
Diff	0.04	0.01	0.06	0.07	0.05	0.10	0.06	0.05	0.07	0.11
HadGEM2										
GFDL	-3.18	-0.55	1.49	0.94	0.29	0.00	0.41	0.39	1.57	0.51 (51.98)
NCAR	-3.14	-0.54	1.58	1.04	0.25	0.11	0.33	0.42	1.65	0.42 (43.00)
Diff	0.04	0.01	0.09	0.09	0.05	0.11	0.07	0.04	0.08	0.09
CanESM2										
GFDL	-3.23	-0.64	1.67	1.03	0.32	-0.21	0.74	0.52	1.83	0.19 (15.18)
NCAR	-3.18	-0.64	1.72	1.07	0.26	-0.10	0.68	0.57	1.87	0.10 (8.38)
Diff	0.04	0.01	0.05	0.04	0.05	0.11	0.06	0.05	0.04	0.08
MIROC5										
GFDL	-3.22	-0.66	1.68	1.02	0.36	-0.22	0.28	0.04	1.38	0.10 (8.50)
NCAR	-3.21	-0.63	1.74	1.11	0.33	-0.11	0.21	0.08	1.47	0.03 (2.36)
Diff	0.01	0.03	0.07	0.09	0.04	0.11	0.07	0.04	0.09	0.07
CCSM4										
GFDL	-3.18	-0.44	1.48	1.05	0.40	-0.27	-0.14	-0.42	1.00	-0.26 (18.51)
NCAR	-3.14	-0.44	1.55	1.11	0.32	-0.13	-0.22	-0.36	1.04	-0.31 (21.85)
Diff	0.05	0.00	0.07	0.06	0.08	0.15	0.09	0.06	0.04	0.05
BNU-ESM										
GFDL	-3.15	-0.22	1.39	1.17	0.48	-0.17	0.28	0.09	1.70	0.28 (39.76)
NCAR	-3.10	-0.23	1.43	1.20	0.39	-0.02	0.22	0.18	1.73	0.20 (28.58)
Diff	0.05	0.01	0.04	0.03	0.09	0.15	0.06	0.09	0.03	0.08
FGOALS-s2										
GFDL	-3.20	-0.53	1.73	1.20	0.37	-0.37	0.28	-0.10	1.43	0.60 (122.58)
NCAR	-3.16	-0.52	1.77	1.25	0.32	-0.26	0.21	-0.06	1.47	0.53 (108.70)
Diff	0.04	0.01	0.04	0.05	0.06	0.11	0.07	0.05	0.03	0.07
MRI-CGCM3										
GFDL	-3.22	-0.61	1.53	0.92	0.37	0.21	-0.00	0.21	1.46	0.11 (8.72)
NCAR	-3.17	-0.60	1.60	1.00	0.32	0.32	-0.09	0.23	1.51	0.06 (4.83)
Diff	0.05	0.01	0.07	0.07	0.05	0.11	0.09	0.02	0.04	0.05
Multimodel mean and intermodel standard deviation										
GFDL	-3.22 (0.04)	-0.60 (0.21)	1.61 (0.14)	1.01 (0.11)	0.34 (0.08)	-0.05 (0.33)	0.28 (0.23)	0.22 (0.42)	1.54 (0.32)	0.19 (0.23)
NCAR	-3.18 (0.05)	-0.60 (0.20)	1.68 (0.14)	1.08 (0.09)	0.28 (0.06)	0.06 (0.32)	0.22 (0.24)	0.27 (0.41)	1.59 (0.33)	0.11 (0.23)
Diff	0.04	0.00	0.06	0.07	0.05	0.11	0.07	0.05	0.06	0.08
Multi-model mean and inter-model standard deviation for the 6 models that exhibit a linear behavior (i.e., $\%Re^\lambda < 10$)										
GFDL	-3.23 (0.03)	-0.67 (0.17)	1.65 (0.12)	0.98 (0.07)	0.31 (0.07)	0.04 (0.41)	0.31 (0.25)	0.34 (0.45)	1.60 (0.37)	0.11 (0.06)
NCAR	-3.20 (0.04)	-0.66 (0.17)	1.71 (0.13)	1.05 (0.06)	0.27 (0.06)	0.14 (0.40)	0.24 (0.26)	0.38 (0.45)	1.66 (0.37)	0.03 (0.06)
Diff	0.03	0.01	0.06	0.07	0.04	0.10	0.07	0.04	0.06	0.08

Table 3 Vertically-integrated (up to tropopause), global and annual mean of feedbacks parameters (in Wm^2K^{-1}) estimated using both the GFDL and NCAR models' radiative kernels, and their multi-model mean and inter-model standard deviation. Also shown for each model, with the same units, is the difference in feedbacks' strength between the two models' kernels. The magnitude of the residual term is also presented (Re^λ , expressed in $Wm^{-2}K^{-1}$ and $\%Re^\lambda$ into brackets, expressed in %), as well as the multi-model mean and inter-model standard deviation for the 6 models that exhibit a linear behavior in the feedback period (for which $\%Re^\lambda < 10$; see also in Section 2.5). Note that the multi-model means and inter-model standard deviations of the residual term is only expressed in $Wm^{-2}K^{-1}$.

267 terms in Eq. 23 to 25 of Soden et al (2008) are not included in the cloud feedback calculation. Note that in Eq.
 268 23 of Soden et al (2008), the change in CRE is constructed from the TOA flux change residual of the clear-sky
 269 feedback factors. In doing so, they assume that the clear-sky change in TOA flux (ΔR^0) can be decomposed into
 270 the sum of clear-sky responses (i.e., $\frac{\Delta R^0}{\Delta T_{s,\Delta sst}} = \sum_x \lambda_x^0$). This might be true for small perturbations, but it is not
 271 necessarily the case when the system is forced beyond $2 \times CO_2$ (Jonko et al, 2012; see also in Table 3 and Section
 272 2.5). Therefore, here, we compute the difference between these two terms as the residual term Re^λ , which is used
 273 to measure the accuracy for the kernel approximation of model-derived clear-sky flux changes for the
 274 abrupt4xCO2 experiment.

275

$$Re^\lambda = \frac{\Delta R^0}{\Delta T_{s,\Delta sst}} - \sum_x \lambda_x^0 \quad (21)$$

276 As for the adjustments, we also express this quantity in percent, which is defined as:

$$277 \%Re^\lambda = \left| \frac{Re^\lambda}{\Delta R^0 / \Delta T_{s,\Delta sst}} \right| \times 100 \text{ (values into brackets in Table 3).}$$

278

279 Vertically-integrated, global and annual mean feedback parameters are shown in Table 3 for each model. For
 280 comparison, and to assess the robustness of our results, the feedbacks have also been computed using the
 281 Geophysical Fluid Dynamics Laboratory (GFDL¹) (Soden et al, 2008) models' kernels. Both the GFDL and
 282 NCAR estimates, as well as their differences are shown in Table 3. On average over the set of models considered
 283 in this study, the two feedback calculations agree to within $\pm 0.1 \text{ W m}^{-2} \text{ K}^{-1}$, and the inter-model spread is the
 284 same for both models' radiative kernels. Larger uncertainties arise for the cloud components, but these are
 285 relatively small compared to the inter-model differences. These results indicate that the use of an alternative
 286 model's kernel does not alter significantly the feedback strength nor its inter-model differences. However,
 287 according to the values of the residual term Re^λ (last column in Table 3), the NCAR models' kernels reproduce
 288 the TOA flux changes more accurately (i.e., $Re^\lambda_{NCAR} < Re^\lambda_{GFDL}$). In the remaining of the paper, all results are
 289 therefore presented for the NCAR models' kernels only.

290

291 2.5 Clear-sky linearity test

292 The radiative kernel technique assumes a linear relationship between TOA radiative changes and the associated
 293 climate responses (i.e., K_x is constant, independent of models and climate states). The applicability of this
 294 method was verified for model responses to forcings of up to $2 \times CO_2$ (Jonko et al, 2012; Shell et al, 2008), but its
 295 adequacy seems reduced when the system is forced by $4 \times CO_2$ and beyond (Block and Mauritsen, submitted;
 296 Jonko et al, 2012). In fact it has been recently shown that the radiative kernels are dependent on the control
 297 state climate and on the magnitude of the forcing (Block and Mauritsen, submitted; Jonko et al, 2012).

298

¹ the GFDL model's kernels are available at <http://metofis.rsmas.miami.edu/~bsoden/data/kernels.html>

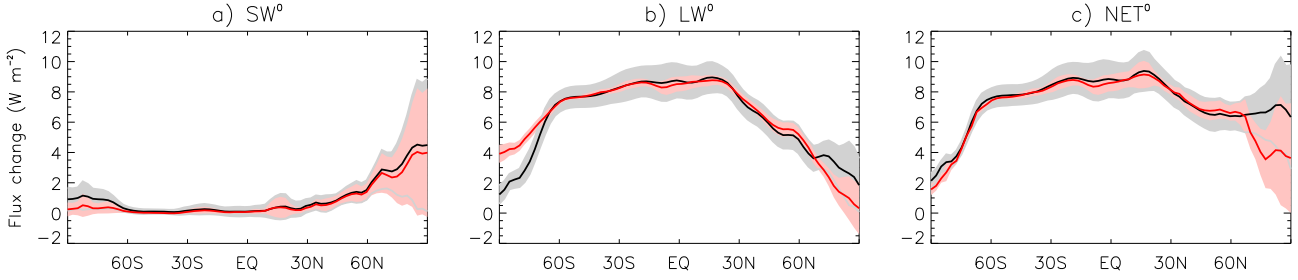
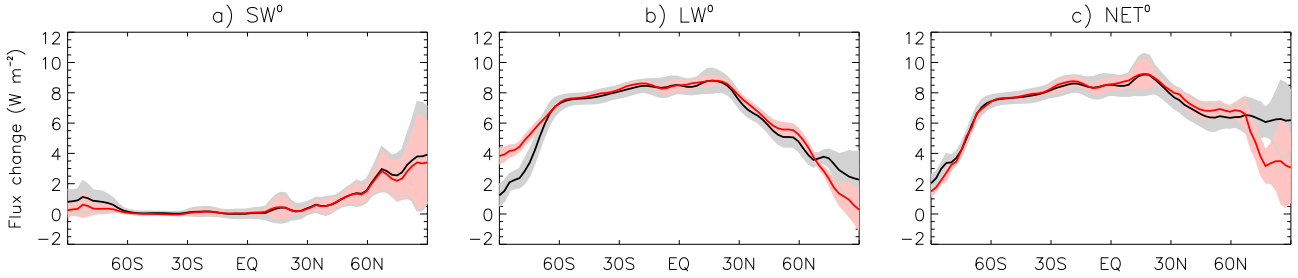
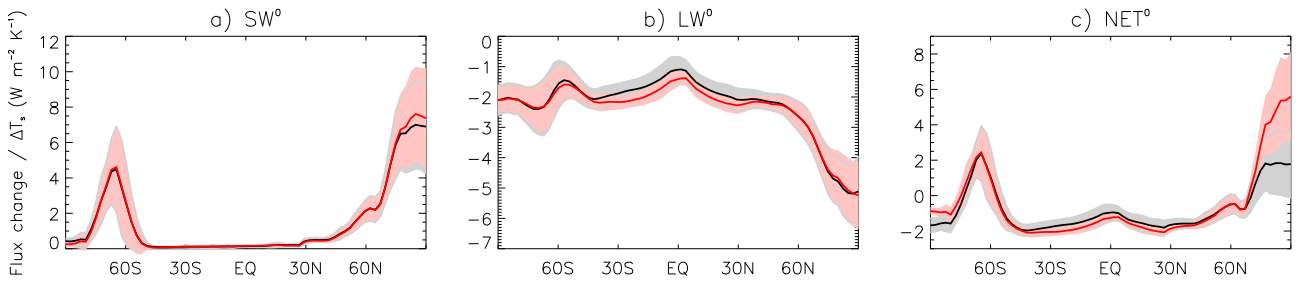
Adjustments to CO_2 : all modelsAdjustments to CO_2 : 8 models that exhibit a linear behavior

Fig. 3 Multi-model mean (solid lines) and inter-model standard deviation (shading) for the change in clear-sky TOA fluxes as derived from model output (ΔR^0 , in black), and for the sum of clear-sky adjustments and forcings derived from the NCAR model's kernels ($\sum_x F_x^0 + G^0$, in red). Zonally-averaged fluxes in Wm^{-2} . Panels (a)-(c) show the SW, LW and NET components for all models. (d)-(f) is for the 8 models that exhibit a linear behavior (for $\%Re^f < 10$ in Table 2).

Feedbacks: all models



Feedbacks: 6 models that exhibit a linear behavior

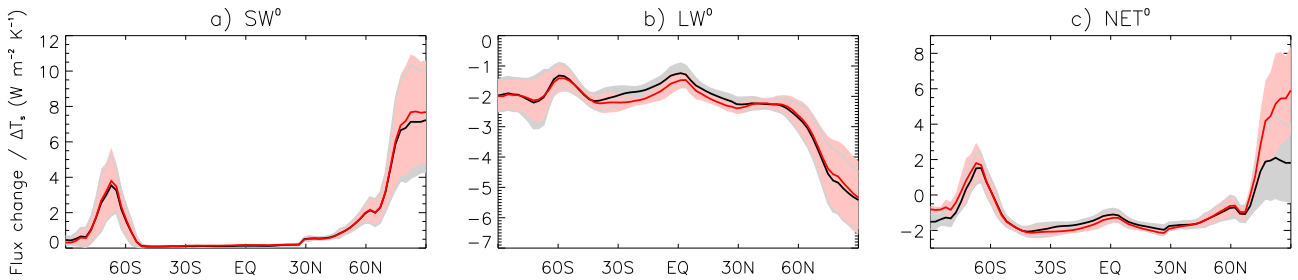


Fig. 4 Same as Figure 3 but for the feedbacks. TOA flux changes derived from model output have been normalized by $\Delta T_s, \Delta SST$ for comparison with the feedbacks. Units are $Wm^{-2}K^{-1}$. (a)-(c) is the SW, LW and NET components for all models, and (d)-(f) is for the 6 models that exhibit a linear behavior (for $\%Re^f < 10$ in Table 3).

299 Here, we test the applicability of the kernel method on our range of climate models, by comparing the changes in
 300 clear-sky TOA radiative fluxes derived from the model simulations and the sum of clear-sky fluxes approximated
 301 by the kernels. This analysis is performed for the zonally-averaged SW, LW and NET components of the
 302 adjustments and forcings (Fig. 3) and the feedbacks (Fig. 4), in addition of the global-averaged residual terms
 303 computed for the adjustments ($\%Re^f$, Table 2) and the feedbacks ($\%Re^\lambda$, Table 3).

304 The linear kernels are considered to be a useful tool for analyzes of feedbacks when the residual term is

comparable to or less than 10% relative to the simulated values (Jonko et al, 2012; Shell et al, 2008). We also use that criterion to test the ability of the kernels to reproduce the global-averaged simulated flux changes in the fixed-SST and the abrupt4xCO2 experiments.

For both the adjustments and the feedbacks, there is a good agreement in the spatial structure of the multi-model mean simulated changes in clear-sky fluxes (black lines) compared to those estimated using the kernels (red lines). However, the magnitude and the inter-model spread of model-derived flux changes are not always well reproduced by the kernels.

For the adjustments (top part of Fig. 3a-c), the NET TOA clear-sky radiative imbalance is positive everywhere and dominated by the LW forcings. A small positive contribution also arises from the SW component between 60°N and 90°N, where there are surface albedo changes due to melting snow and sea-ice as land surfaces warm (Fig. 2c). Values of the residual term for the adjustments, reported for each model in Table 2 ($\%Re^f$), tend to be relatively small, except for three models for which $\%Re^f$ is just above 10% (IPSL-CM5A-LR, CCSM4 and FGOALS-s2). The ability of the kernels to reproduce the global averaged model-derived flux changes, arises, however, from hemispheric compensating errors in the LW component: the kernels systematically overestimate the model-derived flux changes between 60°S and 90°S, while over the Arctic the simulated flux changes are slightly underestimated (Fig. 3b).

For the feedbacks (top part of Fig. 4a-c), the NET clear-sky flux changes are negative everywhere and dominated by the LW component, except over the Arctic and Southern Ocean because of strong SW flux changes associated with decreased surface albedo. There is a systematic difference over the poles, where the net radiative changes, computed using the kernels, are overestimated, while elsewhere they rather tend to be slightly underestimated (Fig. 4c). In most models the kernels overestimate the model-derived SW flux change over the Arctic and Southern Ocean (Fig. 4a). As for the changes in LW flux, the kernels generally underestimate the model-derived values between 30°S and 30°N (Fig. 4b), while no clear tendency emerges at middle and high latitudes because of a large inter-model spread in the differences between the kernel- and the model-derived changes (not shown). We find that the linear kernel analysis is applicable to six models only for the feedback calculation, namely IPSL-CM5A-LR, NorESM1-M, INMCM4, CanESM2, MIROC5 and MRI-CGCM3 (for which $\%Re^\lambda < 10$ in Table 3).

The results presented in Fig. 3 and Fig. 4 also show that the kernel method tends to underestimate the inter-model standard deviation of the changes in clear-sky fluxes (compare the red and grey shadings). The bias introduced by the kernel method essentially affects the clear-sky LW component over the tropics and the mid-latitudes (Fig. 3b and 4b).

We repeated the calculations shown in Fig. 3a-c and 4a-c, but by only using the models that behave linearly, for which $\%Re^f < 10$ and $\%Re^\lambda < 10$, respectively, and we find that the inter-model spread of kernel-derived clear-sky flux changes is now in good agreement with that of model-derived values (bottom part of Fig. 3d-f and Fig. 4d-f).

343 Finally, large deviations from linearity are found in the feedbacks for MPI-ESM-LR (14%), HadGEM2 (43%),
 344 CCSM4 (22%), BNU-ESM (29%), FGOALS-s2 (109%), and in the forcings for IPSL-CM5A-LR (11%), CCSM4
 345 (14%) and FGOALS-s2 (18%), which call into question the robustness of the linear assumption in the calculation
 346 of feedbacks and forcings for those models. Given the results presented in this section, the kernel method might
 347 have quantitative limitations for these models that exhibit a nonlinear behavior, but is qualitatively consistent
 348 with model-derived analysis. In the remaining of the paper, we therefore present our analysis using all models,
 349 but to ensure robustness in our interpretations, we verify our conclusions by restricting our analysis to the
 350 models that exhibit a linear behavior in the forcing or feedback period.

351

352 2.6 Relative contributions of feedbacks and adjustments to climate sensitivity

353 Here, we follow the methodology employed in Dufresne and Bony (2008) to decompose the contributions of the
 354 different feedbacks and adjustments to the equilibrium global temperature change ΔT_s^e .

355 The energy balance in Eq. 9, combined with Eqs. 10-21, separating the Planck feedback from the non-Planck
 356 feedbacks and normalizing by the Planck feedback, can be rewritten as:

$$\Delta T_{s,\Delta sst} = \frac{-1}{\lambda_p} \left[F + F_{adj} - \Delta R + \left(\sum_{x \neq p} \lambda_x + Re^\lambda \right) \Delta T_{s,\Delta sst} \right] \quad (22)$$

357 At equilibrium, when $\Delta R = 0$, it becomes:

358

$$\Delta T_{s,\Delta sst}^e = \frac{-1}{\lambda_p} \left[F + F_{adj} + \left(\sum_{x \neq p} \lambda_x + Re^\lambda \right) \Delta T_{s,\Delta sst}^e \right] \quad (23)$$

359 with $\Delta T_{s,\Delta sst}^e = \frac{F'}{\lambda'}$ (by substituting F and λ for F' and λ' in Eq. 2).

360 Finally, because we consider the radiative changes due to land surface warming as part of the forcings rather than
 361 of the feedbacks (which therefore act to reduce the effective forcing - see Fig. 1), we must add to the equilibrium
 362 global temperature change when the ocean warms in Eq. 23 the contribution from the warming of land surfaces
 363 $\Delta T_{s,0}$. Therefore, the total equilibrium global temperature change is defined as:

$$\Delta T_s^e = \frac{-1}{\lambda_p} \left[F + F_{adj} + \left(\sum_{x \neq p} \lambda_x + Re^\lambda \right) \Delta T_{s,\Delta sst}^e \right] + \Delta T_{s,0} = \Delta T_{s,\Delta sst}^e + \Delta T_{s,0} \quad (24)$$

364 From Eq. 24, we define:

365

366 the Planck response associated with the stratosphere-adjusted forcing (F):

$$\Delta T_{s,F} = -\frac{F}{\lambda_p}, \text{ as in Eq. 4 of Dufresne and Bony (2008)} \quad (25)$$

367 the Planck response associated with all the tropospheric adjustments to CO₂ forcing and land surface warming:

$$\Delta T_{s,F_{adj}} = -\frac{F_{adj}}{\lambda_p} + \Delta T_{s,0} \quad (26)$$

368 More explicitly, this term includes direct adjustments to CO₂ and adjustments to land surface warming
 369 associated with temperature, water vapor, albedo and clouds, the residual for the forcings (Re^f), and the actual
 370 small warming of land surfaces ($\Delta T_{s,0}$, largely compensated by the radiative cooling of the Planck component
 371 F_p).

372

373 the temperature change associated with each feedback parameter x , in response to the atmosphere-adjusted forcing

374 F' :

$$\Delta T_{s,x} = -\frac{\lambda_x}{\lambda_p} \Delta T_{s,\Delta sst}^e \quad (27)$$

375 and the temperature change associated with the feedback residual term Re^λ :

$$\Delta T_{s,Re} = -\frac{Re^\lambda}{\lambda_p} \Delta T_{s,\Delta sst}^e \quad (28)$$

376 such that:

$$\Delta T_s^e = \Delta T_{s,F} + \Delta T_{s,F_{adj}} + \sum_{x \neq p, adj} \Delta T_{s,x} + \Delta T_{s,Re}, \quad (29)$$

377 3 Decomposition of climate sensitivity estimates from CMIP5 models

378 The climate sensitivity estimates of the 11 models considered in this study (as computed from Eqs. 22-29 and
 379 reported in Table 1) range between 1.9 and 4.4 degrees for a doubling of CO₂ concentration. This range is similar
 380 (although slightly lower) to that of CMIP3 (Randall et al, 2007) and to that of CMIP5 diagnosed by Andrews
 381 et al (2012) using a different methodology. Actually, the differences between Andrews et al (2012)'s estimates
 382 and ours remain within $\pm 5\%$ for 7 models that are analyzed in both studies, while one model only (INMCM4)
 383 exhibits a larger difference between the two methodologies (9.5% difference). These results are therefore rather
 384 promising given all the uncertainties involved in estimating the climate sensitivity of models, and the very
 385 different nature of the two methodologies.

386

387 We now analyze the decomposition of equilibrium temperature changes into forcing and feedback terms, as
388 described in section 2.6, for the 11 models (in Table 1). In addition, each contribution to the equilibrium
389 temperature change is separated into three different regions: the tropics (between 30°S and 30°N), the
390 mid-latitudes (between 30° and 60° in each hemisphere) and the poles (between 60° and 90° in each
391 hemisphere). Each regional contribution is weighted by its respective surface area, so that the sum of all regions
392 equals the global value.

393

394 3.1 Multi-model mean analysis

395 The multi-model mean of the equilibrium temperature change ΔT_s , decomposed into regional contributions,
396 feedbacks and into the Planck response of stratosphere-adjusted forcing and adjustments, is shown in Figure 5a.
397 On average over the set of models considered in this study, about 43% of the global warming is associated with
398 the direct response to CO₂ forcing ($\sim 36\%$ for the stratosphere-adjusted forcing and $\sim 7\%$ for the adjustments),
399 and 57% from the feedbacks: $\sim 32\%$ of the warming arises from the combined water vapor + lapse rate (hereafter,
400 WV+LR), $\sim 10\%$ from clouds, $\sim 8\%$ from surface albedo and $\sim 7\%$ from the feedback residual term. When we
401 restrict our analysis to the 6 models for which the residual term is lower than 10% (in Table 3), the contribution
402 to ΔT_s arising from clouds increases up to 14% and that of the residual term becomes less than 3%, while the
403 contribution from the other components changes by at most 2% (not shown). This suggests that errors of
404 nonlinearity introduced by the radiative kernels in the calculation of feedbacks mainly affect the temperature
405 change resulting from the cloud feedback.

406

407 These results are qualitatively similar to those reported by Dufresne and Bony (2008). However, quantitative
408 differences may arise from the fact that cloud adjustments are now included in the forcing term rather than in
409 the feedback term. Indeed, the cloud feedback is found to be 33% weaker on average when the adjustments are
410 considered as part of the forcings rather than of the feedbacks (see section 4.2, where different measures of the
411 cloud feedback are compared). As demonstrated in section 2.1, if the climate sensitivity is not affected by the
412 methodology (this is verified with an uncertainty to within $\pm 3\%$), the feedback parameter, however, is (according
413 to the relation in Eq. 4 and Fig. 1). The total feedback parameter is about 11% stronger (not shown) compared
414 to the previous methodology (Eq. 6).

415 It is interesting to mention that the differences between the adjusted feedback parameters (calculated between
416 sstClim4xCO₂ and abrupt4xCO₂) and the non-adjusted feedbacks (calculated between sstClim and
417 abrupt4xCO₂) - not shown - are rather small for the non-cloud feedbacks (2% difference for the temperature and
418 albedo feedbacks and 6% difference for the water vapor feedback) and for the feedback residual term (5%
419 difference). This suggests that the positive cloud adjustment (as reported in Table 2) is the main component that
420 can alter the feedback parameter, and that the non-cloud adjustments (associated with temperature, water vapor
421 and albedo) seem to be better understood as responses to land surface warming.

422

423 It appears in Figure 5a (left bar) that each latitude belt contributes to global ΔT_s in proportion of its area: the
 424 tropical contribution (between 30°S and 30°N) is $\sim 50\%$, $\sim 35\%$ arises from the mid-latitudes (between 30° and
 425 60° in each hemisphere) and $\sim 15\%$ from polar regions (between 60° and 90° in each hemisphere). Note however
 426 that regional contributions to the inter-model spread are not necessarily proportional to their area extent.

427

428 3.2 Feedback parameters

429 The amplitude of ΔT_s associated with the Planck response (i.e., of stratosphere-adjusted forcing + adjustments,
 430 obtained by summing Eq. 25 and 26) and the feedbacks is shown in Figure 5b. The contributions from the
 431 different regions is also represented for each component, and the sum of all regions (represented by the black
 432 dots) corresponds to the global climate sensitivity estimate (also reported in Table 1).

433 For all models, the contribution to ΔT_s from the Planck response to forcing is the greatest in the tropics (light
 434 grey) and the smallest over the poles (dark grey). A similar tendency is observed for the clouds (in red), the
 435 residual term (in purple) and the combined water vapor + lapse rate feedback (in blue). However, as expected
 436 from sea-ice loss and snow melt with rising temperatures, the albedo feedback is the largest over polar regions
 437 (green shading).

438

439 Inter-model differences occur for each feedback, but those associated with cloud feedbacks are the largest (Fig.
 440 5b). As a result, the spread of climate sensitivity (black dots) is primarily driven by the spread of cloud
 441 feedbacks, especially tropical cloud feedbacks (light red). This is confirmed by the comparison of the normalized
 442 inter-model standard deviation associated with each feedback and each region (Fig. 6a for all models and Fig. 7a
 443 for the 6 models with $\%Re^\lambda < 10$), and by the inter-model regression of the feedbacks against the global mean
 444 temperature change (Fig. 8). These maps of regression slopes indicate the feedbacks and the regions the most
 445 strongly associated with the inter-model spread in climate sensitivity. Figure 8f shows that high sensitivity
 446 models tend to have strong positive cloud feedbacks in the tropics (with contributions from the SW component
 447 in subsidence zones - Fig. 8d, and from the LW component in convective regions - Fig. 8e), but also over the
 448 oceanic basins in the mid-latitudes (because of reduced cloud-albedo effect in the storm track regions - Fig. 8d).

449 Inter-model differences in cloud feedbacks represent about 55% the standard deviation of climate sensitivity in
 450 Fig. 6a. This estimate is substantially reduced as compared to the “70%” reported by Dufresne and Bony (2008),
 451 and this is not due to the fact that tropospheric adjustments to CO_2 are now included in the forcing term rather
 452 than in the feedback term. It is, however, highly sensitive to the feedback residual term (which contributes for
 453 34% to the inter-model standard deviation in ΔT_s in Fig. 6). When we restrict our analysis to the 6 models that
 454 have a small residual term (i.e., $\%Re^\lambda < 10$ in Table 3), its contribution to the inter-model standard deviation in
 455 ΔT_s drops to only 10%, while that of the cloud feedbacks increases up to 70% (Fig. 7a). The tropics is clearly the
 456 region where the spread in cloud feedbacks is the largest ($\sim 48\%$), followed by the mid-latitudes ($\sim 23\%$) and the
 457 poles ($\sim 3\%$).

458 The contribution of WV+LR to the inter-model spread in climate sensitivity, which is the second most
 459 important source of spread in ΔT_s , is lower for the models that have a small residual term ($\sim 30\%$ in Fig. 7a)

460 than when all models are considered ($\sim 40\%$ in Fig. 7a). For this component, the spread also primarily originates
 461 from the tropics, and is mainly driven by the water vapor feedback (Fig. 8b), while the lapse rate feedback tends
 462 to be more strongly associated with the temperature spread over the middle and high latitudes (Fig. 8a).

463 The spread of climate sensitivity arising from the direct response to CO_2 (i.e., stratosphere-adjusted forcing +
 464 adjustments) is less than 15% in Fig. 7a, with the largest contributions in the tropics and the mid-latitudes
 465 ($\sim 6\%$ of ΔT_s in each region). The temperature spread resulting from the surface albedo is the smallest ($< 10\%$
 466 in Fig. 7a), with the largest contribution over polar regions (see also in Fig. 8c).

468 3.3 Adjustments to CO_2 forcing and land surface warming

469 A similar analysis is performed for the Planck response to tropospheric adjustments associated with water vapor,
 470 lapse rate, surface albedo, clouds, and the residual for forcings (Fig. 5c, 6b and 7b). Recall also from Eq. 26 that
 471 there is a contribution from surface temperature, which includes the actual warming of land surfaces ($\Delta T_{s,0}$) and
 472 the Planck response (F_p). We consider those two components together rather than each term individually,
 473 because they are strongly correlated and largely offset each other ($F_p + \Delta T_{s,0}$, in Fig. 5c).

474
 475 The sum of all adjustments produces a small warming ($\Delta T_{s,F_{adj}}$), ranging between 0.04 K and 0.54 K (black
 476 dots in Fig. 5c). No correlation appears between the spread associated with adjustments and that associated
 477 with feedbacks. On average over the 11 models, the largest adjustment arises from the clouds (53% of $\Delta T_{s,F_{adj}}$),
 478 followed by the WV+LR (22%), the albedo (11%), the residual term (8%) and the contribution from land surface
 479 warming (6%). When we only consider the 8 models that have a small residual term (i.e., $\%Re^f < 10$ in Table 2),
 480 there is an increased contribution from the clouds (up to 64% of $\Delta T_{s,F_{adj}}$), which tends to be compensated by a
 481 decreased contribution from the residual term, while the other components remain fairly similar (as also seen in
 482 Table 2). Therefore, similarly to the feedbacks, it seems that the residual term essentially affects the temperature
 483 change associated with cloud adjustments.

484
 485 Although the multi-model mean of the cloud response is the greatest, the residual term constitutes the largest
 486 spread in the amplitude and in the sign of the adjustments (Fig. 5c). The contribution of Re^f to the inter-model
 487 standard deviation in ΔT_s is also the largest among all adjustments, especially in the tropics (Fig. 6b), and this
 488 result remains robust when we restrict the analysis to the 8 models with $Re^f < 10$ (Fig. 7b). Having said that,
 489 the residual term for the forcings only contribute for about 9% of the temperature spread in Fig. 7b, which is
 490 weaker than for any feedback parameter in Fig. 7a. And therefore, the inter-model spread of climate sensitivity
 491 arises primarily from the spread of feedbacks rather than adjustments.

492
 493 The spread resulting from the cloud adjustment is nearly 8% of the inter-model difference in ΔT_s (Fig. 7b). The
 494 tropics contribute the most to the global response in clouds (35% of the multi-model mean for the 8 models with
 495 $\%Re^f < 10$), but it is not the principal source of spread. The tropics and the mid-latitudes contribute almost
 496 equally to the temperature spread (Fig. 7b), while the polar regions constitute the smallest spread.

497 The WV+LR response is weaker than that of the net cloud adjustment (Fig. 5c), with polar regions contributing
498 the most to the global response because of a positive lapse rate response associated with a larger surface warming in
499 these areas, and a relatively small water vapor response in warm regions. Over the tropics and the mid-latitudes the
500 WV+LR adjustment is similar, with a weak but positive (negative) WV (LR) response consistent with the slight
501 land and tropospheric warmings associated with increased CO₂ concentration. Although the greatest WV+LR
502 adjustment is over polar regions, the largest spread is, as for the feedbacks, over the tropics (in Fig. 6b and Fig.
503 7b).

504 The amplitude of adjustment associated with the surface albedo is small, each region contributing equally to the
505 global response, but its contribution to the spread in ΔT_s is comparable to that of the WV+LR adjustment (in
506 Fig. 6b and Fig. 7b), although slightly greater in the tropics and the mid-latitudes. The high tropical surface albedo
507 response (e.g., for models 1 and 9 in Fig. 6b) arises from semi-arid land regions (e.g., over Central Australia, the
508 Sahel - see the multi-model mean in Fig. 2). The adjustment in surface albedo has been further analyzed (not shown)
509 by separating the contribution from the change in incoming SW radiation and the change in reflected SW radiation
510 at the surface, under clear-sky and all-sky conditions. It is found that the incoming flux depends, as expected, on
511 the cloud cover (i.e., with an increase in incoming solar radiation at the surface when the cloud cover decreases,
512 and vice versa), while the reflected flux (which decreases over continental regions in the Northern Hemisphere,
513 the Sahel and central Australia) is the same under clear- and all-sky conditions. This potentially suggests a link
514 between direct or indirect CO₂-induced changes in vegetation, in turn impacting the surface reflectance (Denman
515 et al, 2007).

516 The multi-model mean and inter-model spread resulting from land surface warming ($F_p + \Delta T_{s,0}$) is the smallest
517 in Fig. 5c, 6b and 7b.

518 3.4 Summary

519 Considering climate adjustments to CO₂ does not alter climate sensitivity estimates, but does affect the quantifi-
520 cation of feedbacks. Indeed, the multi-model mean cloud feedback is reduced by about 33%. However, it does not
521 affect the spread of feedbacks. Cloud feedbacks remain the main contribution to the spread of climate sensitivity,
522 especially the tropical cloud feedbacks. To a lesser extent, the tropical WV+LR feedback also contributes to the
523 spread of climate sensitivity estimates. The tropical cloud and WV+LR feedbacks are analyzed further in the next
524 section.

525 Finally, our results point to a substantial role of the residual term in the calculation of adjustments and feedbacks
526 for the interpretation of inter-model spread in climate sensitivity estimates, and caution against the use of methods
527 that include the residual term into one of the linear components (e.g., the cloud feedback of Soden and Held, 2006).

528 4 Analysis of the spread of climate feedbacks in the tropics

529 4.1 The combined water vapor + lapse rate feedbacks

530 In this section we analyze the role of relative humidity (RH) changes to understand the amplitude and the
 531 spread of the tropically-averaged WV+LR feedback seen in Fig. 5 and 6. This is done by following the method
 532 proposed by Soden et al (2008), whereby the water vapor feedback is recomputed by multiplying the water vapor
 533 kernel with the simulated change in atmospheric temperature and assuming no change in simulated RH (see Eq.
 534 20 and 21 of Soden et al (2008) for more details). Hereafter, we refer to this feedback as the fixed-RH WV
 535 feedback (see also Held and Shell, 2012 for an alternative feedback decomposition using relative humidity).

536 Figure 9 shows the tropically-averaged, annual-mean vertical profiles of the WV+LR (a), WV (b) and LR (c)
 537 feedbacks, as well as the fixed-RH WV+LR (d) and WV (e) feedbacks, and the contribution of RH changes to
 538 the WV feedback (computed as the differences: $\lambda_{wv} - \text{fixed-RH } \lambda_{wv}$; this quantity is referred hereafter to as $\tilde{\lambda}_{wv}$,
 539 and is shown in f). As already reported in Soden and Held (2006) and Soden et al (2008), the strength of the
 540 WV feedback is weaker by about 5% than that computed under the assumption of fixed-RH (difference between
 541 the two vertically-integrated global-mean, annual-mean feedbacks - not shown). This difference arises primarily
 542 from the upper troposphere (above 400 hPa - compare Fig. 9b and e), and is consistent with a reduction in
 543 upper-tropospheric relative humidity in all models (as seen in Fig. 9f by negative values of $\tilde{\lambda}_{wv}$). This feature is
 544 robust over the set of models considered in this study. The spread of the WV+LR feedback computed with the
 545 assumption of fixed-RH is considerably reduced throughout the troposphere (Fig. 9d), which confirms that the
 546 spread in WV+LR is mainly controlled by departures from constant relative humidity as simulated by climate
 547 models, and that changes in relative humidity alter the radiative coupling between the water vapor and lapse rate
 548 feedback (Bony et al, 2006). Indeed, the spread of the WV+LR feedback closely follows that of $\tilde{\lambda}_{wv}$ (compare
 549 Fig. 9a and 9f): models with high WV+LR feedback have large increase in RH (and vice versa). This appears
 550 also clearly when we consider the WV+LR feedback plotted as a function $\tilde{\lambda}_{wv}$ over the tropics (Fig. 10): these
 551 two components are well correlated over the tropics, and the spread in WV+LR feedback in this region can be
 552 explained by different changes in RH simulated by the models. Note however that no clear relation arises in the
 553 mid-latitudes, and no change in RH over the poles occur (not shown). The spread of the WV+LR feedback in the
 554 mid-latitudes and the poles can however be explained by inter-model differences in LR feedbacks (not shown).

555 Water vapor in the upper troposphere is recognized as playing a key role in the water vapor feedback (Held and
 556 Soden, 2000). The present results show however that the upper-tropospheric WV and LR feedbacks largely offset
 557 each other, with even a tendency for a greater contribution from the lapse rate resulting in a negative WV+LR
 558 feedback between 300 hPa and 200 hPa (Fig. 9a). Below 300 hPa, however, the contribution from the positive
 559 WV feedback increases up to a maximum near 700 hPa. These results therefore suggest that the positive
 560 WV+LR feedback arises mostly from the mid-troposphere between 500 hPa and 900 hPa.

562 4.2 Cloud feedbacks

563 About 70% of the inter-model spread in climate sensitivity estimates arises from differing cloud feedbacks
 564 (section 3). Although many areas contribute to these differences, the tropics play a prominent role in the spread
 565 of global cloud feedbacks (Figure 7a). In this section, we analyze further the origin of this spread.

566

567 Historically, two main approaches have been used commonly to analyze the response of clouds to climate change:
 568 the diagnostic of cloud feedbacks through Partial Radiative Perturbation (PRP) or kernel approaches (Soden and
 569 Held, 2006; Wetherald and Manabe, 1988), and the change in CRE at the top of the atmosphere (ΔCRE)
 570 between control and perturbed climate states (Cess et al, 1990), which constitutes a much simpler diagnostic. It
 571 is recognized that owing to cloud-masking effects, the sign of ΔCRE can differ from that of the cloud feedback (a
 572 negative ΔCRE being generally associated with a neutral or weakly positive cloud feedback) and that both
 573 measures differ by an offset of about $0.3 \text{ Wm}^{-2}\text{K}^{-1}$ (Soden and Held, 2006; Soden et al, 2004). Besides
 574 cloud-masking effects, how do cloud adjustments to CO_2 alter the relationship between ΔCRE and cloud
 575 feedbacks?

576

577 Figure 11 shows that excluding cloud adjustments from the definition of cloud feedbacks also affects the
 578 magnitude of cloud feedback estimates (compare the star and triangle symbols in Fig. 11). On average over the
 579 set of models considered, the magnitude of the NET cloud feedback is reduced by about 33% when the cloud
 580 adjustments are considered as part of forcing rather than of feedbacks. In addition, cloud feedbacks remain
 581 strongly correlated with the basic ΔCRE (i.e. the ΔCRE not corrected for cloud-masking effects and
 582 adjustments to CO_2), both at the global scale (Fig. 11) and at the tropical scale (Fig. 12). Any of these
 583 diagnostics may thus be considered for analyzing the spread of cloud feedbacks amongst models.

584

585 In the tropics, 6 models predict a positive or neutral cloud feedback (Fig. 12). To understand why some models
 586 have a larger cloud feedback than others, we use the methodology proposed by Bony et al (2004) whereby the
 587 cloud feedback (or CRE sensitivity to surface temperature change, $\frac{\Delta CRE}{T_s}$) is composited into different
 588 dynamical regimes defined from the large-scale mid-tropospheric (500 hPa) vertical velocity (ω). By using this
 589 variable as a proxy of the large-scale tropical circulation (between 30°S and 30°N), we discretize the tropical
 590 geographical pattern into regions of subsidence and ascendance for positive and negative values of ω , respectively.

591

Using this method, the tropically-averaged CRE (\bar{C} , in $\text{Wm}^{-2}\text{K}^{-1}$) can be expressed as:

$$\bar{C} = \sum_{\omega} P_{\omega} C_{\omega}, \quad (30)$$

592 where P_{ω} is the probability of occurrence of regime ω and C_{ω} is the CRE sensitivity in the regime ω .

Now, following Eq. 30, the cloud feedback or CRE sensitivity ($\bar{\Delta C}$) is written as:

$$\bar{\Delta C} = \sum_{\omega} C_{\omega} \Delta P_{\omega} + \sum_{\omega} P_{\omega} \Delta C_{\omega} + \sum_{\omega} \Delta C_{\omega} \Delta P_{\omega}, \quad (31)$$

593 where ΔC_ω and ΔP_ω are the changes in C_ω and P_ω , respectively.

594

595 The first two terms of Eq. 31 quantify CRE changes that arise from large-scale circulation changes (referred to as
 596 the dynamical component), and changes in cloud-radiative properties which are not primarily related to
 597 dynamical changes (referred to as the thermodynamical component), respectively. The third term, which arises
 598 from the co-variation of dynamical and thermodynamical components, is much weaker than the two other terms.
 599 For this reason, the following analysis will be focusing on the dynamical and thermodynamical components.

600 As done by Bony and Dufresne (2005), we group the 11 models into two categories (5 high-sensitivity models and
 601 6 low-sensitivity models) according to their tropically-averaged NET cloud feedbacks or $\Delta CRE/\Delta T_s$
 602 (high-sensitivity models are in red in Fig. 12). Then, the multi-model mean and inter-model spread of the
 603 dynamical and thermodynamical components of the tropical cloud feedback or $\Delta CRE/\Delta T_s$ are computed for
 604 each group. The results being very similar for both measures, and when considering land+ocean regions or ocean
 605 regions only, hereafter we present only the results for the cloud feedback over tropical oceans.

606 Inter-model differences in tropical NET cloud feedbacks primarily arise from the SW component. Figure 13
 607 shows that it is the SW thermodynamical component of the feedback which best discriminates the two groups of
 608 models. All dynamical regimes, from deep convective to subsidence regimes, contribute to these differences.
 609 However, the regimes of weak subsidence and of moderate large-scale rising motion (from -10 to +30 hPa/day)
 610 have a predominant role in the spread, both because these regimes are associated with a larger contrast between
 611 the two groups of models (Fig. 13 left panels), and because of the large statistical weight of these regimes in the
 612 tropics (PDF of ω_{500} , Fig. 13 middle panels).

613

614 To facilitate the comparison between these results and those associated with CMIP3 models, we also compute
 615 the change in CRE predicted by the two groups of models, normalized by the surface temperature change
 616 predicted within each dynamical regime as done by Bony and Dufresne (2005) (Figure 14). As in climate change
 617 the tropical SST does not rise uniformly, the sensitivity of the SW CRE to local rather than global surface
 618 temperature changes is slightly enhanced (reduced) in subsidence (convective) regimes. The comparison of
 619 Figures 13 and 14 also shows the offset of the LW component, and then of the NET ΔCRE , when cloud-masking
 620 effects are not accounted for. Differences in the SW component between the low and high sensitivity groups of
 621 models remain roughly similar, however, although more pronounced in regimes of subsidence.

622

623 Compared to CMIP3, the spread of tropical cloud feedbacks among CMIP5 models thus arises from a larger range
 624 of dynamical regimes, ranging from weak large-scale rising motions to subsidence regimes. Given the predominance
 625 of shallow cumulus and stratocumulus clouds in these regimes, it is likely that the responses of boundary-layer
 626 processes and shallow convection to climate change, and of the different clouds associated with them, constitute
 627 a critical component of the climate sensitivity uncertainty. Although local feedback processes might explain part
 628 of inter-model differences (Zhang and co authors, submitted), the possibility that inter-model differences in cloud-
 629 radiative responses in these regimes be driven by remote responses of deep convection can not be ruled out and
 630 will have to be investigated.

631 5 Conclusion

632 In this paper, we propose an alternative approach to diagnose the radiative forcing, fast adjustments, feedbacks
633 and the climate sensitivity in CMIP5 climate models. We use the NCAR model's radiative kernels (Shell et al,
634 2008) to analyze the different feedbacks and adjustments, by considering tropospheric adjustments to CO_2 and
635 land surface warming as part of forcings rather than feedbacks. The amplitude and inter-model spread of climate
636 sensitivity is quantified, and decomposed into different contributions related to individual adjustments and
637 feedbacks, and into regional contributions. We show that in climate model simulations with large forcing (e.g.,
638 $4 \times CO_2$), nonlinearities in the calculation of adjustments and feedbacks play a non-negligible role for the
639 interpretation of inter-model spread in climate sensitivity estimates (also consistent with Jonko et al, 2012's
640 findings). We therefore caution against the use of methods in which nonlinearities are assumed minor and
641 included into one of the linear components (e.g., the cloud feedback of Soden and Held, 2006).

642 Taking into account the tropospheric adjustments to CO_2 does not affect the estimate of climate sensitivities.
643 For a doubling of CO_2 concentration, the equilibrium global-mean temperature change estimates range from 1.9
644 to 4.4 degrees. This range is similar to that of CMIP3 (Randall et al, 2007) and to that diagnosed by Andrews
645 et al (2012) for CMIP5 models using a different methodology. On the other hand, considering tropospheric
646 adjustments to CO_2 does alter the quantification of feedbacks. The total feedback parameter is increased by
647 about 11% compared to the previous methodology in which the adjustments to CO_2 were included in the
648 feedbacks rather than in the forcing. The cloud feedback is the most affected, with a reduction of about 33%
649 relative to the previous method's estimates, while the non-cloud adjustments (associated with temperature,
650 water vapor and albedo) seem to be better understood as responses to land surface warming. The effect of cloud
651 adjustments on feedbacks is qualitatively consistent but quantitatively weaker than found by Andrews and
652 Forster (2008) using a different methodology to diagnose feedbacks. Moreover, and unlike Andrews and Forster
653 (2008), the consideration of the adjustments to CO_2 does not reduce the inter-model spread of feedbacks
654 amongst CMIP5 models. Cloud feedbacks remain the main contributors to the spread of climate sensitivity,
655 especially tropical cloud feedbacks. The tropical combined water vapor + lapse rate feedback also contributes
656 substantially to the spread of climate sensitivity, although to a lesser extent.

657 Further analysis of the tropical combined water vapor + lapse rate feedback shows that changes in relative
658 humidity, as simulated by climate models, affect the radiative coupling between the water vapor and lapse rate
659 feedback. The spread of the tropical combined water vapor + lapse rate feedback is entirely due to different
660 simulated changes in relative humidity throughout the troposphere.

661 Like in CMIP3, the spread of tropical cloud feedbacks primarily arises from differing changes in the shortwave
662 cloud-radiative properties in regions of shallow convection (where shallow cumulus and stratocumulus clouds
663 prevail), which in turn result from changes in the thermodynamic structure of the tropical atmosphere.
664 Interpreting this spread in terms of local and remote physical processes and using observations to assess the
665 relative reliability of the different model responses clearly remains a scientific challenge for the years to come.
666 However, the wealth of CMIP5 experiments and output now available constitutes a wonderful opportunity to
667 make progress on that matter.

669 **References**

- 670 Andrews T, Forster P (2008) CO₂ forcing induces semi-direct effects with consequences for climate feedback
671 interpretations. *Geophys Res Lett* 35:L04,802
- 672 Andrews T, Gregory J, Webb M, Taylor K (2012) Forcing, feedbacks and climate sensitivity in CMIP5 coupled
673 atmosphere-ocean climate models. *Geophysical Research Letters* 39(9):L09,712
- 674 Block K, Mauritsen T (submitted) Forcing and feedback in the MPI-ESM-LR coupled model under abruptly
675 quadrupled CO₂. *Journal of Geophysical Research*
- 676 Boer G, Yu B (2003) Climate sensitivity and climate state. *Climate dynamics* 21(2):167–176
- 677 Bony S, Dufresne J (2005) Marine boundary layer clouds at the heart of tropical cloud feedback uncertainties in
678 climate models. *Geophysical Research Letters* 23:L20,806
- 679 Bony S, Dufresne JL, Treut HL, Morcrette JJ, Senior C (2004) On dynamic and thermodynamic components of
680 cloud changes. *Climate Dynamics* 22:71–86
- 681 Bony S, Colman R, Kattsov V, Allan R, Bretherton C, Dufresne J, Hall A, Hallegatte S, Holland M, Ingram W,
682 et al (2006) How well do we understand and evaluate climate change feedback processes? *Journal of Climate*
683 19(15):3445–3482
- 684 Bony S, Stevens B, Held I, Mitchell J, Dufresne JL, Emanuel K, Friedlingstein P, Griffies S, Senior C (2013, in
685 press) Carbon dioxide and climate : Perspectives on a scientific assessment. *Climate Science for Serving Society:*
686 *Research, Modelling and Prediction Priorities*, J Hurrell and G Asran Editors, Springer Monograph
- 687 Bony S, Bellon G, Klocke D, Fermepin S, Sherwood S, Denvil S (submitted) Direct effect of carbon dioxide on
688 tropical atmospheric circulation and regional rainfall. *Nature Geoscience*
- 689 Cess R, Potter G, Blanchet J, Boer G, Del Genio A, Deque M, Dymnikov V, Galin V, Gates W, Ghan S, et al
690 (1990) Intercomparison and interpretation of climate feedback processes in 19 atmospheric general circulation
691 models. *Journal of Geophysical Research* 95(16):601,216
- 692 Charney JG, et al (1979) Carbon dioxide and climate: a scientific assessment : report of an Ad Hoc Study Group
693 on Carbon Dioxide and Climate, Woods Hole, Massachusetts, July 23-27, 1979 to the Climate Research Board,
694 Assembly of Mathematical and Physical Sciences, National Research Council. National Academy of Sciences :
695 available from Climate Research Board, URL <http://books.google.com/books?id=cj0rAAAAYAAJ>
- 696 Colman R, McAvaney B (2011) On tropospheric adjustment to forcing and climate feedbacks. *Climate dynamics*
697 36(9):1649–1658
- 698 Denman K, Brasseur G, Chidthaisong A, Ciais P, Cox P, Dickinson R, Hauglustaine D, Heinze C, Holland E,
699 Jacob D, et al (2007) Couplings between changes in the climate system and biogeochemistry. *Climate Change*
700 2007: The Physical Science Basis Contribution of Working Group I to the Fourth Assessment Report of the
701 Intergovernmental Panel on Climate Change [Solomon, S, D Qin, M Manning, Z Chen, M Marquis, KB Averyt,
702 MTignor and HL Miller (eds)]
- 703 Dufresne JL, Bony S (2008) An assessment of the primary sources of spread of global warming estimates from
704 coupled atmosphere-ocean models. *Journal of Climate* 21:5135–5144
- 705 Forster P, Ramaswamy V, Artaxo P, Berntsen T, Betts R, Fahey D, Haywood J, Lean J, Lowe D, Myhre G, et al
706 (2007) Changes in atmospheric constituents and in radiative forcing. *Climate Change 2007: The Physical Science*

- 707 Basis Contribution of Working Group I to the Fourth Assessment Report of the Intergovernmental Panel on
708 Climate Change [Solomon, S, D Qin, M Manning, Z Chen, M Marquis, KB Averyt, MTignor and HL Miller
709 (eds)]
- 710 Gregory J, Webb M (2008) Tropospheric adjustment induces a cloud component in CO₂ forcing. *Journal of Climate*
711 21:58–71
- 712 Gregory JM, Ingram WJ, Palmer MA, Jones GS, Thorpe PASRB, Lowe JA, Johns TC, Williams KD (2004) A
713 new method for diagnosing radiative forcing and climate sensitivity. *Geophysical Research Letters* 31:L03,205
- 714 Hansen J, Sato M, Ruedy R, Nazarenko L, Lacis A, Schmidt G, Russell G, Aleinov I, Bauer M, Bauer S, et al
715 (2005) Efficacy of climate forcings. *Journal of Geophysical Research* 110(D18):D18,104
- 716 Held I, Soden B (2000) Water vapor feedback and global warming 1. *Annual Review of Energy and the Environment*
717 25(1):441–475
- 718 Held IM, Shell KM (2012) Using relative humidity as a state variable in climate feedback analysis. *Journal of*
719 *climate* 25(8):2578–2582
- 720 Jonko A, Shell K, Sanderson B, Danabasoglu G (2012) Climate feedbacks in CCSM3 under changing CO₂ forcing.
721 part I: Adapting the linear radiative kernel technique to feedback calculations for a broad range of forcings.
722 *Journal of Climate* 25(15):5260–5272
- 723 Knutti R, Hegerl G (2008) The equilibrium sensitivity of the earth’s temperature to radiation changes. *Nature*
724 *Geoscience* 1(11):735–743
- 725 Mauritsen T, Graverson RG, Klocke D, Langen PL, Bjorn S, Tomassini L (submitted) Climate feedback efficiency
726 and synergy. *Climate Dynamics*
- 727 Randall D, Wood R, Bony S, Colman R, Fichet T, Fyfe J, Kattsov V, Pitman A, Shukla J, Srinivasan J, et al
728 (2007) Climate models and their evaluation. *Climate change* 323
- 729 Shell KM, Kiehl JT, Shields CA (2008) Using the radiative kernel technique to calculate climate feedbacks in
730 NCAR’s community atmospheric model. *Journal of Climate* 21:2269–2282
- 731 Soden B, Held I (2006) An assessment of climate feedbacks in coupled ocean-atmosphere models. *Journal of Climate*
732 19(14):3354–3360
- 733 Soden B, Held I, Colman R, Shell K, Kiehl J, Shields C (2008) Quantifying climate feedbacks using radiative
734 kernels. *Journal of Climate* 21(14):3504–3520
- 735 Soden BJ, Broccoli AJ, Hemler RS (2004) On the use of cloud forcing to estimate cloud feedback. *Journal of*
736 *Climate* 19:3661–3665
- 737 Taylor KE, Stouffer RJ, Meehl GA (2012) An overview of CMIP5 and the experiment design. *Bulletin of the*
738 *American Meteorological Society* 93(4):485–498, DOI 10.1175/BAMS-D-11-00094.1
- 739 Webb M, Senior C, Sexton D, Ingram W, Williams K, Ringer M, McAvaney B, Colman R, Soden B, Gudgel R,
740 et al (2006) On the contribution of local feedback mechanisms to the range of climate sensitivity in two GCM
741 ensembles. *Climate Dynamics* 27(1):17–38
- 742 Wetherald RT, Manabe S (1988) Cloud feedback processes in a general circulation model. *Journal of Atmospheric*
743 *Sciences* 45:1397–1415

744 Zhang M, co authors (submitted) CGILS: First results from an international project to understand the physical
745 mechanisms of low cloud feedbacks in general circulation models. Bulletin of American Meteorological Society

746 **Acknowledgements** The research leading to these results has received funding from the European Union, Seventh Framework
747 Programme (FP7/2007-2013) under grant agreement n° 244067 for the EUCLIPSE project, and under GA 226520 for the COM-
748 BINE project. The work was also partially funded by the ANR ClimaConf project. We acknowledge the World Climate Research
749 Programme's Working Group on Coupled Modelling, which is responsible for CMIP, and we thank the climate modeling groups
750 (listed in Table 1 of this paper) for producing and making available their model output. For CMIP the U.S. Department of
751 Energy's Program for Climate Model Diagnosis and Intercomparison provides coordinating support and led development of soft-
752 ware infrastructure in partnership with the Global Organization for Earth System Science Portals. The authors would like to
753 acknowledge Karen Shell and Brian Soden for making the NCAR and GFDL models' radiative kernels freely available online at
754 <http://people.oregonstate.edu/~shellk/kernel.html>. Finally, we thank Christelle Castet for her participation to this study, and
755 we acknowledge the anonymous reviewers for their helpful comments and suggestions.

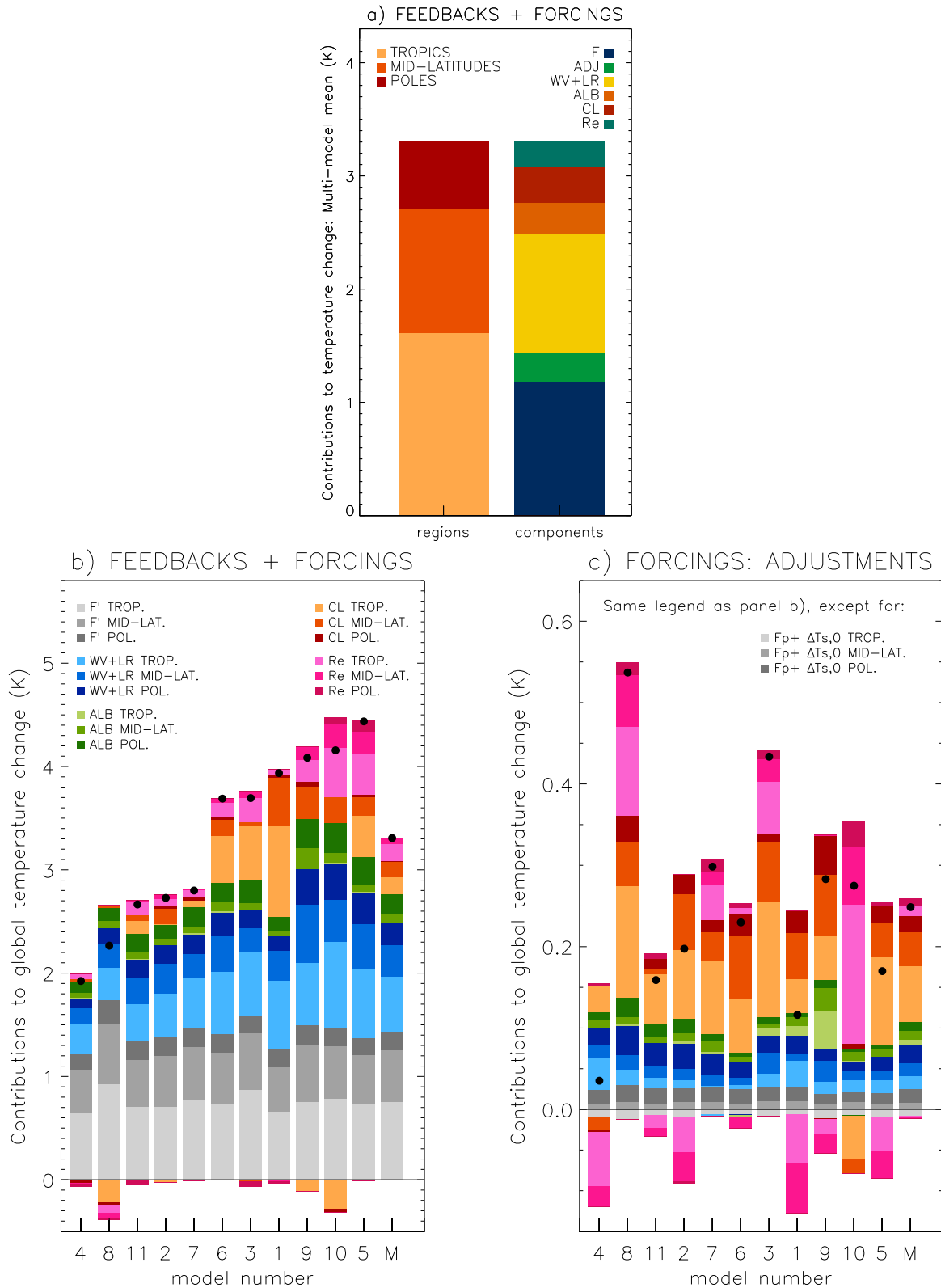


Fig. 5 (a) multi-model mean of the climate sensitivity estimate ΔT_s , separated into regional contributions from the tropics (between 30°S and 30°N), the mid-latitudes (between 30° and 60° in each hemisphere) and the poles (between 60° and 90° in each hemisphere) (left) and into its different components, including the Planck response to stratosphere-adjusted forcing (F, Eq. 25), the Planck response to the adjustments to CO_2 forcing and land surface warming (ADJ, Eq. 26), the combined water vapor + lapse rate (WV+LR), the albedo (ALB), the cloud (CL) feedbacks (Eq. 27) and the feedback residual term (Re^λ , Eq. 28) (right). (b) climate sensitivity estimates (as indicated by the black dots) associated with the Planck response to the stratosphere-adjusted forcing and the adjustments (F' , in grey - obtained by summing Eq. 25 and Eq. 26), the combined water vapor + lapse rate feedback (WV+LR, in blue), the albedo feedback (ALB, in green), the net cloud feedback (CL, in red) and the feedback residual term (Re, in purple), computed for each of the 11 models listed in table 1. $\Delta T_{s,F} + \Delta T_{s,F_{adj}}$, $\Delta T_{s,x}$ and $\Delta T_{s,Re}$'s are also decomposed into the three different regions: the tropics (light shading), the mid-latitudes (medium shading) and the poles (dark shading). (c) global mean surface temperature change (as indicated by the black dots) associated with the Planck response to land surface warming (F_p) + $\Delta T_{s,0}$ (grey), the adjustments for the combined water vapor + lapse rate (blue), the albedo (green), the net cloud adjustments (red) and the residual term (purple). The models are sorted according to increasing ΔT_s , and model numbers correspond to the listing in Table 1. The last column (M) in panels (b) and (c) correspond to the multi-model mean for the feedbacks and adjustments, respectively. Note the different scales of the temperature change (y-axis) among each panel.

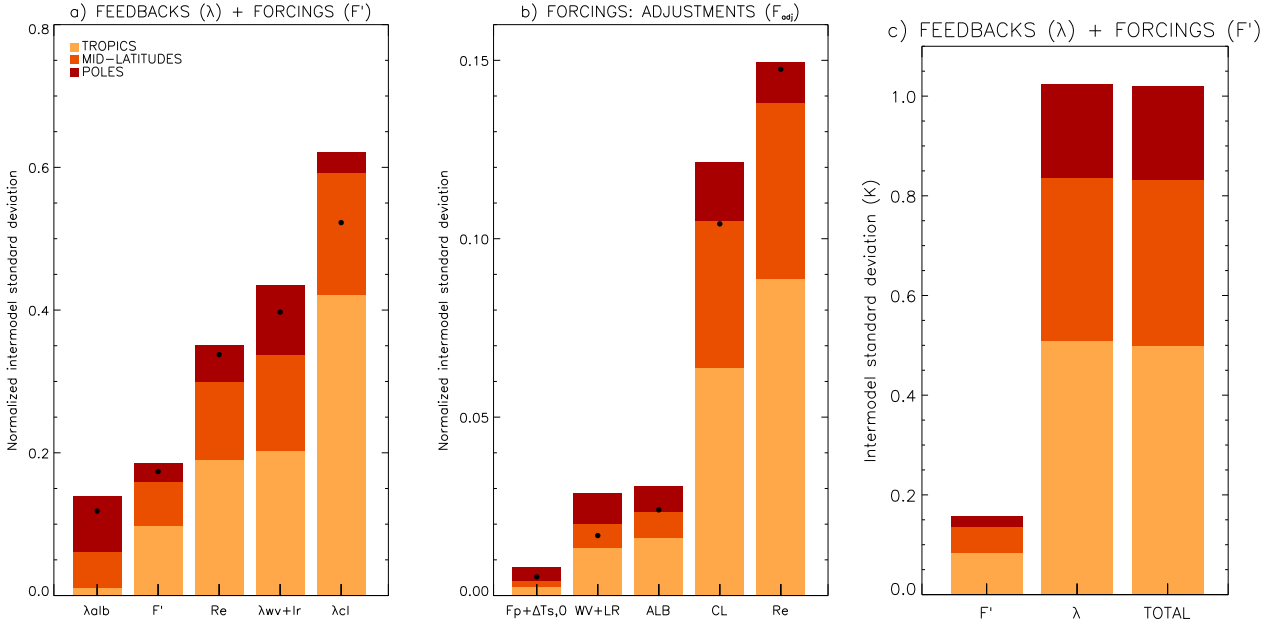
All models:

Fig. 6 (a) Inter-model standard deviation of climate sensitivity estimates associated with the atmosphere-adjusted forcing (which includes the Planck response to the stratosphere-adjusted forcing and to the adjustments) and the feedbacks in each region, normalized by the inter-model standard deviation of ΔT_s (no units). Note that for this metrics, the contributions from the different regions are not additive, and the normalized inter-model standard deviation of ΔT_s over the globe is reported as black dots. (b) same as (a), but for the Planck response to the adjustments only. (c) Inter-model standard deviation of climate sensitivity estimates (in Kelvin) associated with the atmosphere-adjusted forcing (which includes the Planck response to the stratosphere-adjusted forcing and to the adjustments) and the feedbacks (λ). The last bar (TOTAL) is the inter-model standard deviation of ΔT_s associated with both the forcing and the feedbacks. Note the different scales and units on the y-axis among each panel. Note also that, unlike it appears in panel (c), the regional contributions to the inter-model standard deviation are not necessarily proportional to their area extent.

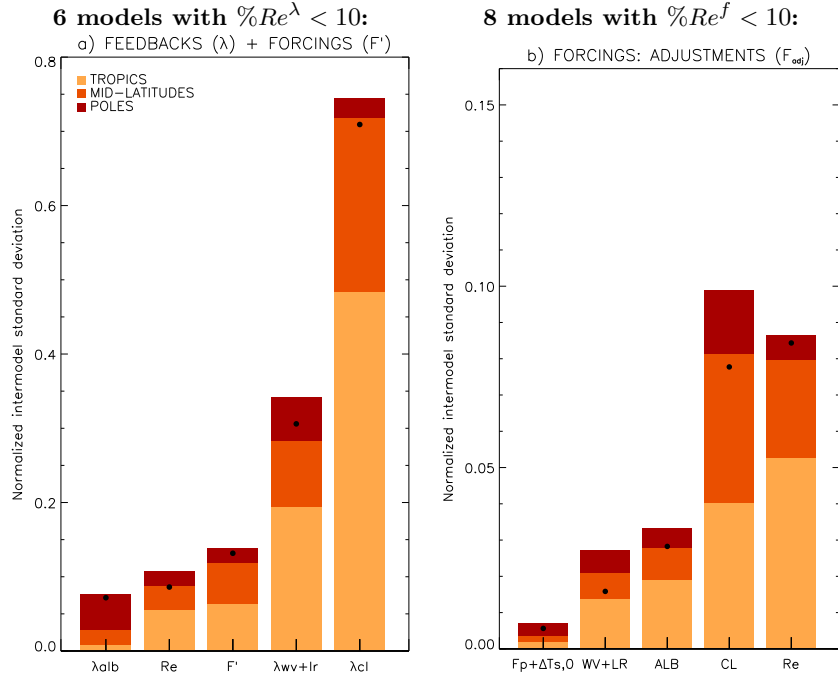


Fig. 7 (a) Same as Figure 6a, but for the 6 models for which the residual for the feedbacks $\%Re^\lambda < 10$ (see Table 3). (b) Same as Figure 6b, but for the 8 models for which the residual for the adjustments $\%Re^f < 10$ (see Table 2).

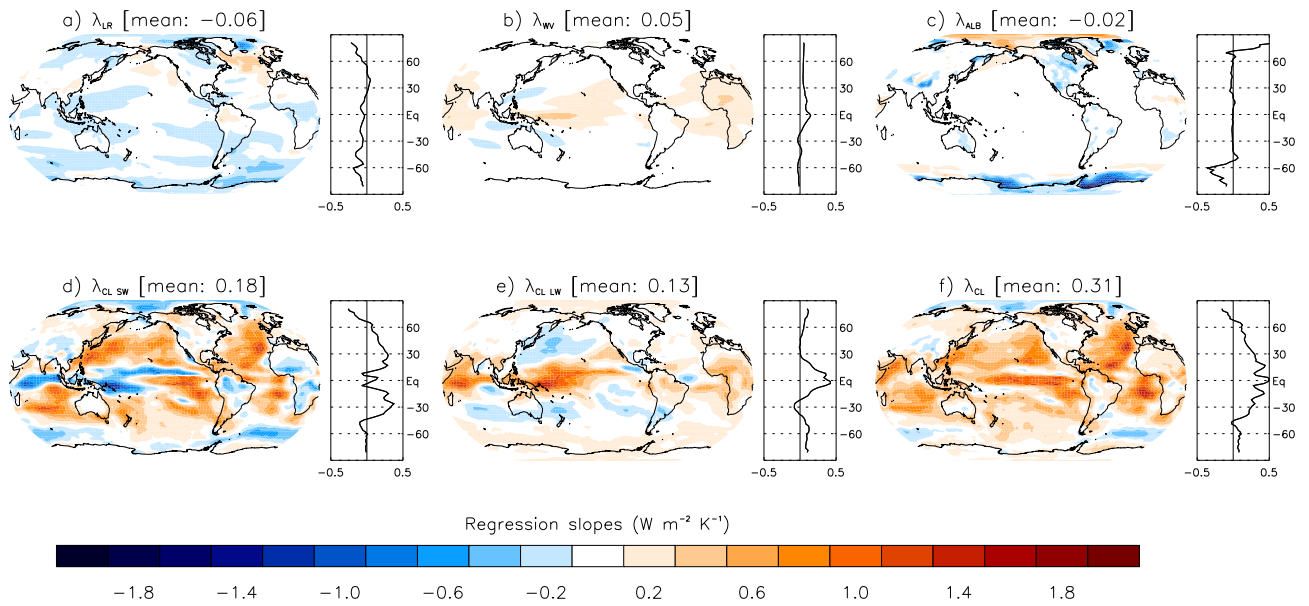


Fig. 8 Inter-model regression slopes of the lapse rate (a), water vapor (b), albedo (c) and cloud (SW in d; LW in e; NET in f) feedbacks against the global mean surface temperature change for the 11 models considered in this study and reported in Table 1. Large values indicate the regions where the feedbacks are the most strongly associated with the inter-model spread in climate sensitivity.

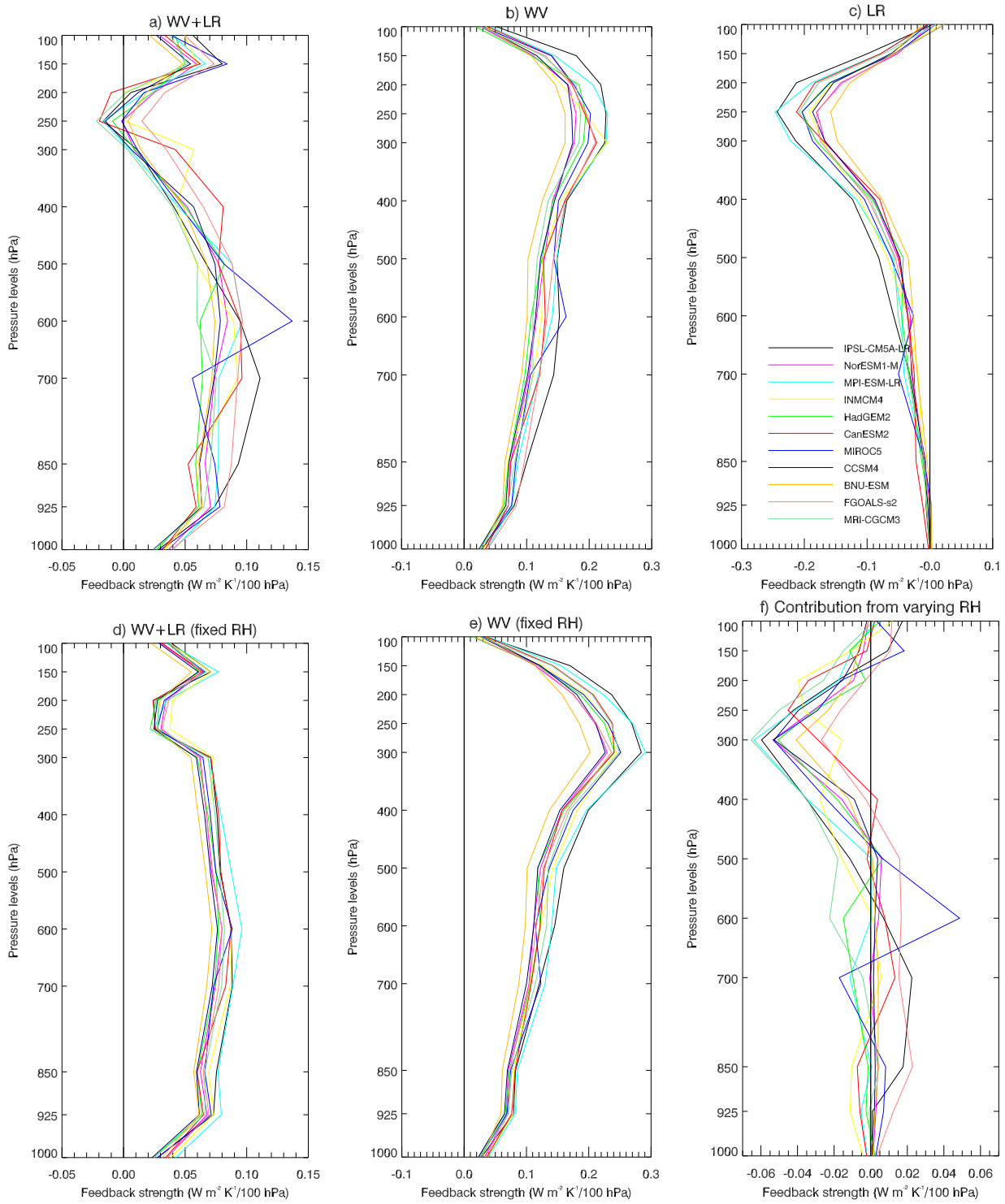


Fig. 9 Tropically-averaged, annual-mean vertical profile of the WV+LR (a), WV (b), LR (c), WV+LR (assuming fixed RH, d), WV (assuming fixed RH, e) feedbacks and the contribution of the WV feedback arising from changes in RH (f).

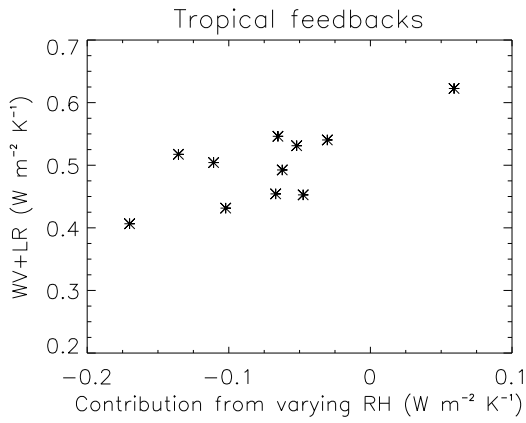


Fig. 10 Vertically-integrated, tropically-averaged, annual mean WV+LR feedback for the 11 models plotted as a function of the vertically-integrated, tropically-averaged, annual mean contribution of RH changes to the WV feedback.

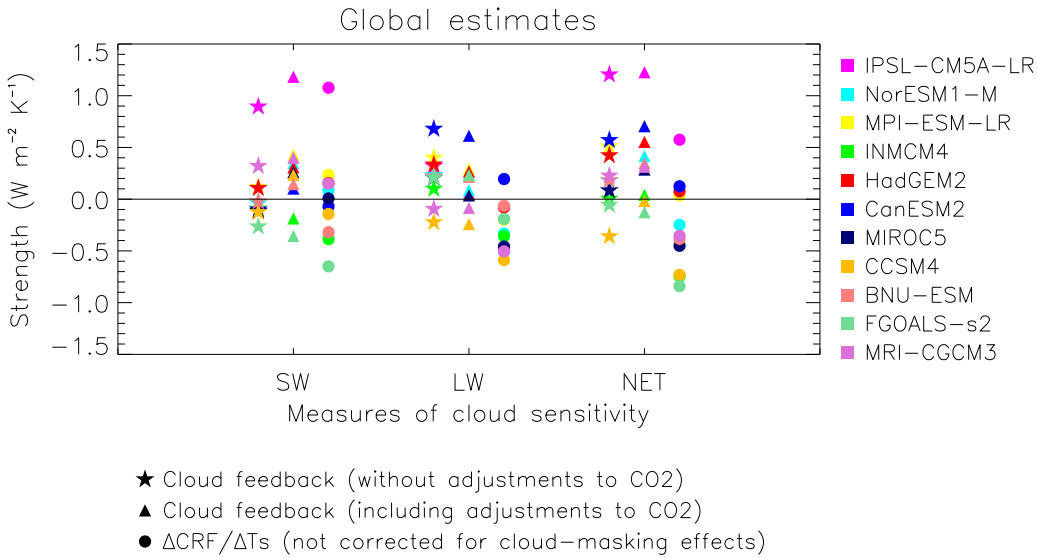


Fig. 11 Global and annual mean of three cloud sensitivity measures for the SW, LW and NET components computed for the set of models considered: the cloud feedback computed, using the NCAR model’s radiative kernels, by considering the adjustments to CO₂ as part of the forcing rather than the feedbacks (stars), the cloud feedbacks that include the adjustments to CO₂ (triangles), and the changes in CRE, normalized by ΔT_s, that include the adjustments to CO₂ and that are not corrected for cloud-masking effects (circles).

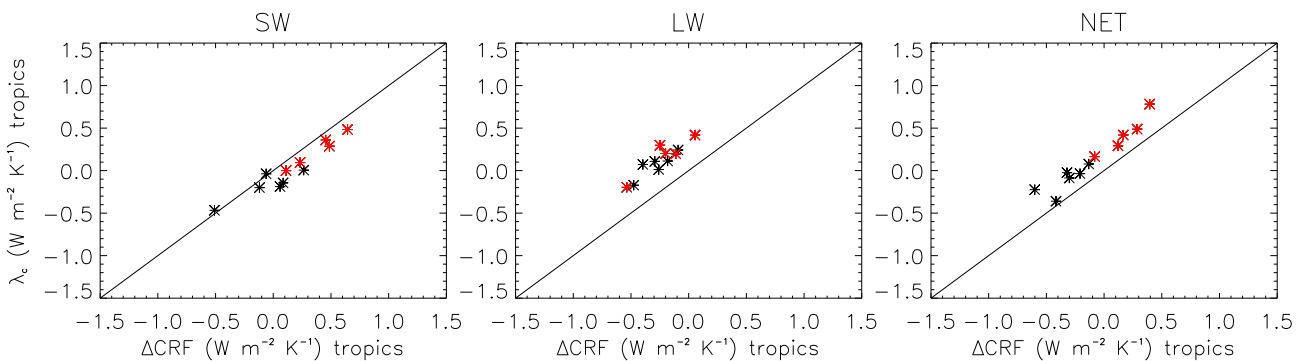


Fig. 12 Tropically-averaged cloud feedback parameter (estimated using the NCAR kernels) plotted as a function of the change in cloud radiative effect (i.e., including cloud adjustments, and without correction of the cloud-masking effect) normalized by the global mean surface temperature change over the tropics. Models that predicts a greater tropically-averaged NET cloud sensitivity (i.e., cloud feedback or change in CRE) than the tropically-averaged multi-model mean NET cloud sensitivity are shown in red (5 models), and those predicting a lower cloud sensitivity than the multi-model mean are in black (6 models)

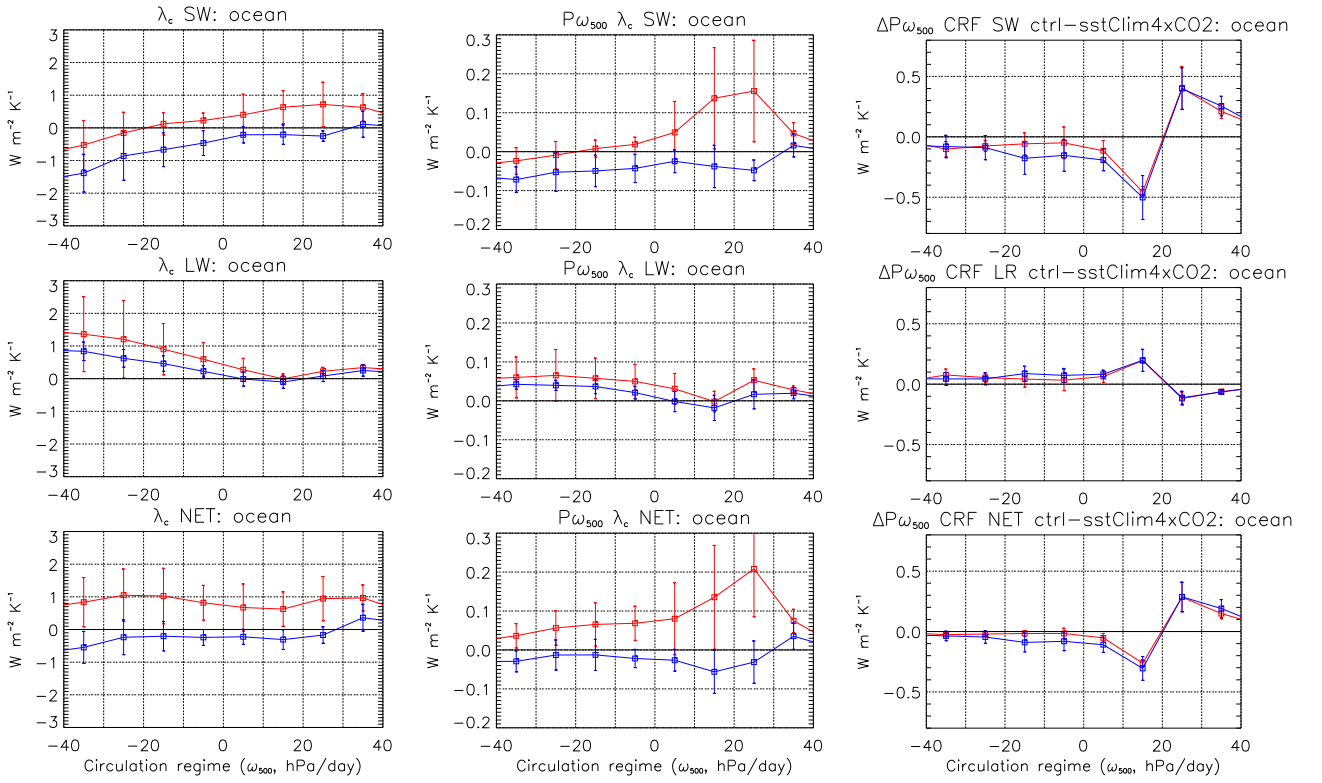


Fig. 13 SW (top), LW (middle) and NET (bottom) cloud feedback ($\bar{\Delta C}$) composited in each dynamical regime (left), the contribution from the thermodynamic component ($P_\omega \Delta C_\omega$, middle) and from the dynamic component ($C_\omega \Delta P_\omega$, right). Results are presented for two groups of models: models that predicts a greater tropically-averaged NET cloud feedback than the tropically-averaged multi-model mean NET cloud feedback (in red, 5 models), and those with a lower cloud sensitivity than the multi-model mean (in blue, 6 models). Vertical bars show the inter-model standard deviation in each group. Cloud feedbacks are estimated using the NCAR model's radiative kernels.

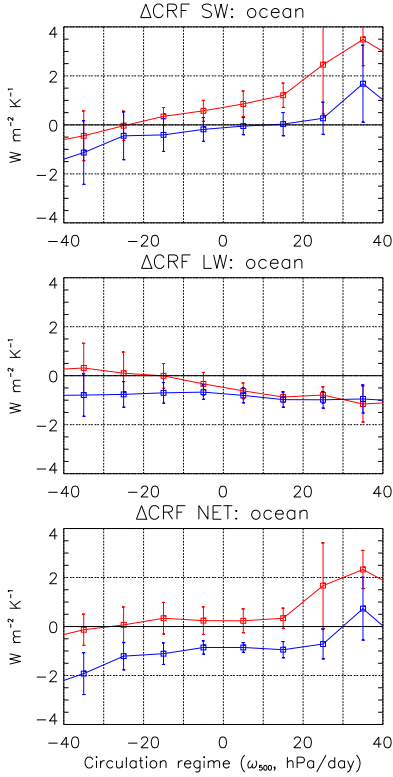


Fig. 14 Same as the left panel of Figure 13, but for the change in CRE, normalized by the mean surface temperature change in the regime ω . The models that predict a greater change in the tropically-averaged NET CRE than its multi-model mean are in red (i.e., multi-model mean for this group), and models that predict a lower change are in blue.